Chemical Engineering Journal 523 (2025) 168162

Contents lists available at ScienceDirect

Chemical Engineering Journal

journal homepage: www.elsevier.com/locate/cej

A new method for estimating the globally averaged mass transfer coefficient in liquid-particle agitated vessels

Ziming Wang, Luca Mazzei *

Department of Chemical Engineering, University College London, Torrington Place, London WC1E 7JE, UK

ARTICLE INFO

Keywords:
Turbulent liquid-particle suspensions
Mass transfer coefficients
Agitated vessels
CFD
Turbulent multifluid model

ABSTRACT

This work focuses on estimating the globally averaged mass transfer coefficient in liquid-particle agitated vessels. After discussing how this coefficient is defined and calculated, we review the main methods for deriving its correlations, namely the dimensional analysis, steady-state theory, unsteady-state theory, and Kolmogorov theory methods. These rely on simplifying assumptions that limit their accuracy, such as the possibility of neglecting the effects of particle interactions and free-stream turbulence on mass transfer. To overcome these limitations, we propose a new method that obtains the global mass transfer coefficient by averaging the local mass transfer coefficient over the entire fluid domain. To determine the local mass transfer coefficient field, we adopt a new model that accounts for the combined effects of fluid-particle slip velocity, particle interactions and free-stream turbulence on mass transfer. The fields of the required fluid dynamic variables are obtained using a validated turbulent multifluid model. The proposed approach is validated against selected experimental datasets covering a wide range of operating conditions. Compared to existing methods, our method yields significantly improved accuracy, with relative errors below 30% for most cases.

1. Introduction

Mass transfer between liquids and particles is critical in many industrial applications, such as adsorption, crystallization and extraction. In these applications, agitated vessels are commonly employed to suspend the particles and enhance mass transfer between the phases. In general, the mass transfer rate within a vessel is quantified using a globally averaged mass transfer coefficient $\overline{k}$, or its dimensionless equivalent, a globally averaged Sherwood number $\overline{\mathrm{Sh}}$, which is usually correlated with the physical properties and fluid dynamic variables of the system. However, in agitated vessels, the fluid dynamic variables are inherently nonuniform and the flow is usually turbulent; therefore, estimating $\overline{k}$ accurately is challenging.

To estimate $\overline{k}$ in agitated vessels and develop suitable correlations, several methods have been proposed, including those based on dimensional analysis and the steady-state, unsteady-state and Kolmogorov theories. Among these, the first considers the globally averaged mass transfer coefficient directly, whereas the others start by considering the mass transfer coefficient for a generic particle within the vessel and then relate it to the globally averaged mass transfer coefficient.

Studies based on the dimensional analysis theory use the Buckingham theorem to find the dimensionless groups characterizing the mass transfer process in agitated vessels, such as $\overline{\mathrm{Sh}}$, the Reynolds number and the Schmidt number [1–7]. After, they use experimental data to correlate these dimensionless groups. But certain important dimensionless groups may be overlooked; furthermore, the correlations are often case-specific, with different forms found (for the same system) in different studies. In addition, geometric similarity, typically required by this method [8], may be absent in some studies, potentially leading to inaccuracies.

The steady-state theory calculates the mass transfer coefficient of a generic particle within a vessel using correlations for isolated particles derived under the assumption that away from the particle the fluid velocity of approach is uniform and constant (that is, the fluid-particle slip velocity, or free-stream velocity, is fixed) [9–12]. Correlations of this type are those by Frossling [13] and Friedlander [14]. These require knowledge of the slip velocity between the fluid and the particle in question. To obtain this, Kuboi et al. [10] solved the Tchen equation [15], assuming that fluid-mediated particle–particle interactions are negligible; for dense suspensions, this assumption may cause inaccuracies. Moreover, in agitated vessels fluid dynamic variables are nonuniform, leading to varying slip velocities among the particles. However, solving the Tchen equation for each particle to obtain all the corresponding slip velocities is impractical; accordingly, Kuboi et al. [10] assumed that the slip velocity is equal for all the particles in the vessel and, using this value in the correlations for isolated

* Corresponding author.
E-mail address: l.mazzei@ucl.ac.uk (L. Mazzei).

https://doi.org/10.1016/j.cej.2025.168162
Received 19 May 2025; Received in revised form 13 July 2025; Accepted 5 September 2025
Available online 19 September 2025

particles, estimated the globally averaged mass transfer coefficient (which therefore coincides with the mass transfer coefficient of each individual particle). This simplification may also reduce accuracy. Alternatively, Hartmann et al. [11] and Hormann et al. [12] estimated the slip velocity for each particle by using the Discrete Particle Modeling (DPM) method and calculated the mass transfer coefficients for all the particles. But these studies did not extend their analysis to the globally averaged mass transfer coefficient; furthermore, this approach is computationally demanding, being viable only for systems with relatively small numbers of particles. Moreover, this theory suffers from a few additional limitations. On the one hand, agitated vessels usually contain dense suspensions, where the presence of other particles affects the mass transfer process for a specific one; consequently, correlations for isolated particles may be inapplicable, and those that consider this effect are required [16–19]. On the other hand, in agitated vessels the flow is usually turbulent, and the free-stream velocity is not uniform or constant but fluctuates rapidly. Under these conditions (that is, in the presence of free-stream turbulence), eddies from the fluid bulk penetrate the laminar boundary layers around the particles, causing fluctuations in velocity and concentration, thereby enhancing mass transfer [20,21]; nonetheless, the correlations mentioned above do not account for this effect.

To capture the effect of free-stream turbulence, researchers have proposed the unsteady-state theory, on which various approaches have been developed. One identifies the relevant dimensionless groups associated with mass transfer for a fixed particle in a turbulent flow, with the turbulence in the free stream statistically uniform and steady; besides the dimensionless groups present in the absence of free-stream turbulence, the most important additional group is the free-stream turbulence intensity, defined as the ratio between the root mean square of the fluid velocity fluctuations and the mean fluid velocity in the free stream (e.g., [21–26]). Using experimental data of mass transfer coefficients for this system, these studies modify the correlations adopted by the steady-state theory. But all these works are limited to fixed isolated particles, and the applicability of these modifications to agitated vessels, where both liquid and particles are in motion and many particles are involved, remains untested.

Another approach solves the Reynolds-averaged boundary layer equations, where the averaging process introduces additional terms associated with turbulent dispersion. The resulting mean concentration profile near the fluid-solid interface is then used to derive the mass transfer coefficient (e.g., [20]). However, studies using this approach have focused only on flat plates and cylinders, and no correlations have been developed for spherical particles.

A third method based on the unsteady-stated theory models the mass transfer process via the penetration theory, which assumes that eddies continuously bring small fluid elements from the bulk of the liquid to the fluid-solid interface and vice versa; these remain at the interface for a certain time during which unsteady diffusion dominates mass transfer (e.g., [9,10,27–30]). This method leads to correlations involving the Kolmogorov eddy dissipation rate [10,30]. Because in agitated vessels this rate is nonuniform, in general the mass transfer coefficient is different for each particle. But similarly to what we discussed for the steady-state theory, several studies neglect this variation, assuming for all the particles an equal mass transfer coefficient based on the mean dissipation rate [10,30]. This is a simplification that might generate inaccuracies. In addition, the penetration theory assumes a uniform velocity distribution near the particle surface, which is justified for bubbles but certainly not for (solid) particles.

Studies based on the Kolmogorov theory regard the root mean square of the relative velocity between two points in a turbulent flow, denoted as u', as the effective velocity for mass transfer, employing it in mass transfer coefficient correlations [30–34]. As for the steady-state theory, this approach typically adopts correlations for isolated particles, neglecting the effects of the surrounding particles. Furthermore, u' depends on the distance between the two selected points; this distance is generally assumed to be equal to the particle diameter, a choice without a strong theoretical basis. Moreover, u' is a function of the Kolmogorov eddy dissipation rate, and thus for different particles in the vessel its value varies. Nevertheless, as for similar works based on the unsteady-state theory, these studies usually assume that u', and in turn the mass transfer coefficient, is equal for all the particles, and use the average dissipation rate to compute the globally averaged mass transfer coefficient. In addition, some studies have considered several influential factors and modified the correlations; for instance, Levins and Glastonbury [32] accounted for the effects of the ratio between the densities of the particle and the liquid and for the ratio between the diameters of the vessel and the impeller, while Bong et al. [34] considered the effect of the solid volume fraction. But these modifications are often case-specific and may not apply when system conditions change.

In conclusion, this section has highlighted some limitations of the available methods for estimating the globally averaged mass transfer coefficient in agitated vessels. To overcome these limitations, we propose a new method that integrates the multiphase fluid dynamics in the vessel, predicted using a turbulent multifluid model, and the effects of fluid-particle slip velocity, particle interactions and free-stream turbulence on mass transfer. The article is structured as follows: Section 2 briefly reviews the definition and calculation of the globally averaged mass transfer coefficient; Section 3 discusses the available theories for developing its correlations; Section 4 describes the methodology employed in this study; finally, Section 5 validates the proposed approach by comparing its predictions with experimental data.

2. Definition and calculation of the coefficient

In this section, we define the globally averaged mass transfer coefficient in agitated vessels and describe how it is calculated from experimental data.

2.1. Definition of the coefficient

Let us consider an agitated vessel containing an isothermal fluid-particle suspension composed of a Newtonian liquid and uniformly sized spherical particles with equal density. In the literature, the globally averaged mass transfer coefficient between the particles and the liquid in the vessel, denoted as $\overline{k}$, is generally defined using the following equation:

$$\frac{dM_V}{dt} \equiv A_V \overline{k}(C_s - \overline{C}) \tag{2.1}$$

Here, dM_V/dt and A_V denote the global mass transfer rate between the liquid and the particles and the total surface area of the particles, respectively. C_s is the saturation concentration at the particle surface, while $\overline{C}$ is the mean solute concentration in the vessel, which changes owing to mass transfer. If all the particles are suspended, A_V can be calculated using the globally averaged solid volume fraction $\overline{\alpha}_s$ as follows:

$$A_V = 6\overline{\alpha}_s V_V / d_p \tag{2.2}$$

Here, V_V is the total volume of the suspension, whose variation due to mass transfer is generally neglected, and d_p is the particle diameter. As summarized in Table 1, in the experiments usually one uses ion exchange beads or dissolving particles. For the former, d_p and $\overline{\alpha}_s$ typically change negligibly, while for the latter, they both change during the experiment. Moreover, individual particles may exhibit different mass transfer rates, leading to a distribution in particle diameter; but capturing this variability is complex, so it is often assumed that all the particles have identical size. Combining Eqs. (2.1) and (2.2) yields:

$$\frac{dM_V}{dt} = \frac{6\overline{\alpha}_s V_V}{d_p}\overline{k}(C_s - \overline{C}) \tag{2.3}$$

Using this equation, three approaches have been proposed to derive analytical expressions for $\overline{k}$, which can be used to obtain the value of $\overline{k}$ experimentally. These will be discussed in the following section.

Table 1
Summary of the experimental conditions of liquid-particle mass transfer coefficient measurement in agitated vessels.

Reference	Liquid	Particles	Impeller type	d_V (cm)	H/d_V	d_I/d_V	C_I/d_V	$d_p(mm)$	$\overline{\alpha}_{s,0}(\%)$	Sc	N (rpm)
Hixson and Wilkens [35]	Water, sperm, cottonseed, and rapeseed oil	Benzoic acid	Propeller-4	15–61	1	0.33	0.17	6.35	0.88–2.96	485–$2.5 \cdot 10^6$	88–500
Hixson and Baum [1]	Water, benzene, and ethylene glycol	Benzoic acid and rock salt	Propeller-4	15–119	1	0.33	0.17	6.35	14.5	776	89–353
Humphrey and Van Ness [2]	Water	Sodium thiosulfate pentahydrate (cylindrical shape)	Propeller-3 and FBT-6	30.48	1	0.33	0.25	*NA*	*NA*	*NA*	200–1300
Nagata et al. [4]	Gelatine, polyviny lalcohol, sucrose and glycerine in water, hydrogen chloride and aqueous solutions	Zn, $AgNO_3$, $KMnO_4$, $K_2Cr_2O_7$, NaCl, NH_4NO_3, NH_4Cl, H_3BO_3, $CO(NH_2)_2$, phenylacetic acid and crotonic acid	45°, 75° and 90° paddles-4	10–30	1	0.5	0.4	0.111–2.27	0.01–0.29	100–$5 \cdot 10^4$	175–800
Barker and Treybal [3]	Water and sucrose solution	Boric acid, rock salt and benzoic acid	DT-6	15–46	0.99–1	0.25–0.67	0.33	0.93–5.45	1.54–10.3	958–$6.2 \cdot 10^4$	57–13412
Harriott [9]	HR solution, HR in meghocel solution, HR in glycerine solution, dextrose solution, water, and HCl solution	Benzoic acid, butyl-benzoic acid, boric acid, lead sulfate, zinc, and ion exchange beads	DT-6	10–54	0.93–1.75	0.25–0.5	0.23–0.46	0.008–7.88	6.4	518–$1.27 \cdot 10^5$	52–1046
Sykes and Gomezplata [6]	Potassium iodide and iodine in water and sucrose solution	Copper	Propeller-3, DT-6, FDT and 45° paddle-6	13.46	1.13	0.47	0.33, 0.5	3.175	0.15	770–$1.13 \cdot 10^4$	250–650
Nienow [36]	Water	K_2SO_4, NH_4Cl, alum, and salt	DT-6	14	1	0.26–0.52	0.14–0.33	0.2–8.8	0.89–4.37	441–1839	63–2046
Kuboi et al. [10]	Water	Ion-exchange resin	DT-6	10.5	1	0.5	0.33	0.25–0.94	*NA*	*NA*	380–3600
Nienow [37]	Water	NaCl	DT-6, FBT-2, and PTD-4	14–28	1	0.25–0.75	0.17–0.5	2.23	17.83	649	79–1700
Boon-Long et al. [7]	Water	Benzoic acid	DT-6	9–63	1	0.33	0.5	2.9	0.0001–0.05	943	25–176
Lal et al. [38]	Water, glycol, and cellulose solutions	Benzoic acid	FBT-2, DT-(2-6), and propeller-4	14.5–25	1	0.22–0.67	0.33	5.13–20.08	0.18–0.22	772	0.98–2440
Armenante and Kirwan [30]	NaOH solution, NaOH in glycerol solution, and $AgNO_3$ in $NaNO_3$ solution	Ion exchange beads	DT-6	19	1.07	0.33	0.36	0.001–0.43	0.009–0.046	547–$1.3 \cdot 10^5$	81–970
Jadhav and Pangarkar [39]	Water and cellulose solution	Benzoic acid	DT-4, FBT-4, and FBT-6	15–57	1	0.33	0.13–0.33	0.0005–1.1	0.39	800	251–960
Bong [40]	NaOH solution	Ion exchange beads	DT-6	20–30	1	0.33	0.25	0.67	0.6–40	669	352–611
Carletti et al. [41]	Water	NaCl	DT-6, A310-3, and PTD-6	23–48	1.18	0.31–0.42	0.33	3	0.008	1000	22–807

DT = disk turbine, PTD = pitched-blade turbine (downflow), FBT = flat-blade turbine, FDT = fan disk turbine, A310 = Lightnin A310 turbine. The number after the impeller type is the blade number. '*NA*' denotes the related data is unavailable.

2.2. Calculation of the coefficient

To derive an analytical expression for $\overline{k}$, most experimental studies determine dM_V/dt by measuring how $\overline{C}$ varies in time [3,6,9,30,34]. In this case, Eq. (2.3) is rewritten as:

$$\frac{dM_V}{dt} = V_V \frac{d[(1-\overline{\alpha}_s)\overline{C}]}{dt} = \frac{6\overline{\alpha}_s V_V}{d_p}\overline{k}(C_s - \overline{C}) \tag{2.4}$$

For ion exchange beads, because their size changes negligibly, $\overline{\alpha}_s$ and d_p are replaced by their initial values, denoted as $\overline{\alpha}_{s,0}$ and $d_{p,0}$, respectively. Often, this is also done for dissolving particles, even if $\overline{\alpha}_s$ and d_p vary over time. This is justified when $\overline{k}$ is measured over a short time interval in which only a small fraction of the particles dissolves [3]. For experiments where particles fully dissolve, this assumption may lead to inaccurate results.

Furthermore, $\overline{k}$ is usually assumed to be constant, even if during the experiments in general mass transfer makes the liquid and particle properties change. But for sufficiently short experiments, this approximation is also acceptable. Then, integrating Eq. (2.4) from the initial state to time τ yields:

$$\ln\frac{C_s - \overline{C}_\tau}{C_s - \overline{C}_0} = -\left[\frac{6\overline{\alpha}_{s,0}\overline{k}}{(1-\overline{\alpha}_{s,0})d_{p,0}}\right]\tau \tag{2.5}$$

where $\overline{C}_0$ and $\overline{C}_\tau$ are the globally averaged solute concentrations at time zero and time τ, respectively. By measuring $\overline{C}_\tau$ over time, one can use the above equation to estimate $\overline{k}$. However, $\overline{C}_\tau$ is generally measured at a single point in the vessel, assuming that the solute is uniformly distributed (i.e., well mixed) in the vessel. As noted by Montante et al. [42], this assumption is reasonable for dilute suspensions in lab-scale vessels, but may be inaccurate for dense suspensions or large-scale vessels. Furthermore, some studies (for instance, Barker and Treybal [3] and Bong et al. [34]) omitted the term $1/(1-\overline{\alpha}_{s,0})$, even for dense suspensions; therefore, their results may have to be corrected.

As described, the method above does not account for variations in particle diameter and volume fraction. For dissolving particles, these variations may be significant. To overcome this, two other methods have been adopted. One obtains dM_V/dt by measuring how the total particle mass M_s changes in time [36,37,43,44], expressing Eq. (2.3) as:

$$\frac{dM_V}{dt} = -\frac{dM_s}{dt} = -V_V\rho_s\frac{d\overline{\alpha}_s}{dt} = \frac{6\overline{\alpha}_s V_V}{d_p}\overline{k}(C_s - \overline{C}) \tag{2.6}$$

where ρ_s is the particle density. The total volume of the suspension V_V is assumed to be constant, while d_p is related to $\overline{\alpha}_s$ as follows:

$$\frac{d_p}{d_{p,0}} = \left(\frac{\overline{\alpha}_s}{\overline{\alpha}_{s,0}}\right)^{1/3} \tag{2.7}$$

Substituting Eq. (2.7) into Eq. (2.6) results in:

$$\frac{d\overline{\alpha}_s}{dt} = -\left[\frac{6\overline{\alpha}_{s,0}^{1/3}\overline{k}(C_s - \overline{C})}{\rho_s d_{p,0}}\right]\overline{\alpha}_s^{2/3} \tag{2.8}$$

Due to mass transfer, $\overline{C}$ is time-dependent, so an analytical solution cannot be derived. But if $\overline{C} \ll C_s$ or if $\overline{C}$ changes minimally during the dissolution process, Eq. (2.8) yields:

$$\left(\frac{\overline{\alpha}_{s,\tau}}{\overline{\alpha}_{s,0}}\right)^{1/3} = \left(\frac{M_{s,\tau}}{M_{s,0}}\right)^{1/3} = 1 - \left[\frac{2\overline{k}(C_s - \overline{C})}{\rho_s d_{p,0}}\right]\tau \tag{2.9}$$

where $\overline{\alpha}_{s,\tau}$ and $M_{s,\tau}$ are the solid volume fraction and total solid mass at time τ, respectively, while $M_{s,0}$ is the initial mass of the solid. Eq. (2.9) allows estimating $\overline{k}$ by measuring the total solid mass over time [44]. Furthermore, for cases where particles fully dissolve, once $M_{s,\tau}$ reaches zero, the second term on the right-hand side of Eq. (2.9) equals unity, so $\overline{k}$ can be estimated by measuring the dissolution time. For cases where the particle size varies substantially, this approach is more rigorous than the previous one (Eq. (2.5)) but holds only if $\overline{C} \ll C_s$ or if $\overline{C}$ changes minimally.

To account for variations in particle diameter and solid volume fraction, Grisafi et al. [45] introduced the globally averaged concentration assuming complete dissolution of all particles, denoted as $\overline{C}_d$ (note that $\overline{C}_d$ may exceed C_s). $\overline{C}_d$ is related to $\overline{C}_0$ and $\overline{C}$ via the following mass conservation equation:

$$M_{s,0} + V_e\overline{C}_0 = M_s + V_e\overline{C} = V_e\overline{C}_d \tag{2.10}$$

in which V_e is the liquid volume, assumed by the authors to be constant during the dissolution process. Then, Eq. (2.10) is rewritten as:

$$\frac{M_s}{M_{s,0}} = \frac{\overline{C}_d - \overline{C}}{\overline{C}_d - \overline{C}_0} \tag{2.11}$$

Substituting this into Eq. (2.6) leads to:

$$\frac{d\overline{C}}{dt} = \Psi\left(\frac{\overline{C}_d - \overline{C}}{\overline{C}_d - \overline{C}_0}\right)^{2/3}\overline{k}(C_s - \overline{C}) \quad ; \quad \Psi \equiv \frac{6(\overline{C}_d - \overline{C}_0)}{\rho_s d_{p,0}} \tag{2.12}$$

where Ψ is a constant of known value. Integrating Eq. (2.12) from time zero to time τ, and assuming that $\overline{k}$ is constant, yields:

$$\frac{1}{2}\ln\left[\left(\frac{1-y_s}{y_\tau - y_s}\right)^3\left(\frac{y_\tau^3 - y_s^3}{1-y_s^3}\right)\right] + \sqrt{3}\arctan\left(\frac{2y_\tau + y_s}{\sqrt{3}y_s}\right) - \sqrt{3}\arctan\left(\frac{2+y_s}{\sqrt{3}y_s}\right) = y_s^2\Psi\overline{k}\tau \tag{2.13}$$

where:

$$y_s \equiv \left(\frac{\overline{C}_d - C_s}{\overline{C}_d - \overline{C}_0}\right)^{1/3} \quad ; \quad y_\tau \equiv \left(\frac{\overline{C}_d - \overline{C}_\tau}{\overline{C}_d - \overline{C}_0}\right)^{1/3} \tag{2.14}$$

For $\overline{C}_\tau \ll C_s$, Eq. (2.13) reduces to Eq. (2.9). Moreover, Eq. (2.13) is valid only for $y_s \neq 0$ (i.e., for $\overline{C}_d \neq C_s$); if these concentrations are equal, the solution reads:

$$y_\tau = [1 - (2/3)\Psi\overline{k}\tau]^{-1/2} \tag{2.15}$$

If the values of $\overline{C}_0$, $\overline{C}_d$, C_s and Ψ are known, by measuring the function $\overline{C}_\tau$ one may obtain $\overline{k}$. But note that the above derivation assumes that the liquid volume changes negligibly; moreover, the challenges associated with measuring $\overline{C}_\tau$, as discussed below Eq. (2.5), still exist.

In summary, we have reviewed three methods for experimentally calculating the globally averaged mass transfer coefficient. Each involves certain assumptions and simplifications. The first method is less accurate when the particle size changes significantly, for it uses the initial values of the particle size and solid volume fraction. Although the other two methods account for changes in these variables, the second method applies only when $\overline{C} \ll C_s$ or when $\overline{C}$ changes negligibly, while the third neglects changes in the liquid volume. In addition, all three methods assume that $\overline{k}$ is constant, an assumption which is reasonable when measurements are conducted over a sufficiently short time interval but that may introduce uncertainties when measurements span the entire mass transfer process.

3. Methods for developing correlations for the coefficient

As discussed in Section 1, many methods have been proposed for obtaining correlations for the globally averaged mass transfer coefficient in agitated vessels; these include the dimensional analysis theory, the steady-state theory, the unsteady-state theory and the Kolmogorov theory. Among them, only the first considers $\overline{k}$ directly, while the others start from evaluating the mass transfer coefficient k_i for a generic particle i and then relate it to $\overline{k}$. Below, Section 3.1 reviews the steady-state, unsteady-state and Kolmogorov theories methods, which are adopted to develop correlations for k_i, while Section 3.2 discusses how k_i can be related to $\overline{k}$, concluding by reviewing the dimensional analysis approach.

3.1. Mass transfer coefficient for isolated particles

3.1.1. Steady-state theory

In the literature, when the slip (or relative) velocity between the fluid and a generic particle i, denoted as $u_{r,i}$, is uniform and constant (i.e., in the absence of free-stream turbulence), the correlations for the mass transfer coefficient k_i usually have the form:

$$\mathrm{Sh}_i = 2 + C_c \mathrm{Re}_i^p \mathrm{Sc}^q \quad ; \quad \mathrm{Sh}_i \equiv k_i d_p / \mathscr{D} \quad ; \quad \mathrm{Re}_i \equiv u_{r,i} d_p / \nu_e \quad ; \quad \mathrm{Sc} \equiv \nu_e / \mathscr{D} \tag{3.1}$$

Here, the constant 2 accounts for mass transfer owing to molecular diffusion under zero flow conditions. Sh_i is the Sherwood number for the particle, Sc is the Schmidt number, and Re_i is the particle Reynolds number, characterized by the fluid-particle slip velocity $u_{r,i}$. $\mathscr{D}$ is the molecular diffusivity of the solute, and ν_e is the kinematic viscosity of the fluid. C_c, p, and q are constants; their values depend on the assumptions adopted in deriving the correlation. Two popular correlations, based on the laminar boundary layer theory, are those by Friedlander [14], for $\mathrm{Re}_i \ll 1$ ($C_c = 0.991$, $p = q = 1/3$), and Frossling [13], for $\mathrm{Re}_i \gg 1$ ($C_c = 0.552$, $p = 1/2$, $q = 1/3$). In the latter case, although turbulence may arise beyond the separation point due to the large values of the local Reynolds number, the wakes contribute negligibly to mass transfer [13] – a behavior distinctly different from that induced by free-stream turbulence.

3.1.2. Unsteady-state theory

To account for the effect of free-stream turbulence, several methods have been used, including those based on the dimensional analysis, boundary layer and penetration theories.

Dimensional analysis method

In this method, one first identifies the parameters characterizing the mass transfer process for a particle in a turbulent flow and then applies the Buckingham theorem to find the relevant dimensionless groups [21–26]. In addition to the dimensionless groups shown in Eq. (3.1), two others, characterizing turbulence, are introduced: the dimensionless turbulence integral length scale L_i and the turbulence intensity T_i. The former, defined as the ratio between the turbulence integral length scale and the particle diameter, is usually neglected, because it plays a minor role; the key quantity that affects mass transfer is the latter, which, for a fixed particle in a turbulent stream, is defined as:

$$\mathrm{T}_i \equiv \frac{1}{|\langle \bar{\boldsymbol{u}}_{r,i} \rangle|} \sqrt{\frac{\langle (\bar{\boldsymbol{u}}_{r,i} - \langle \bar{\boldsymbol{u}}_{r,i} \rangle)^2 \rangle}{3}} \tag{3.2}$$

where $\bar{\boldsymbol{u}}_{r,i}$ is the (instantaneous) velocity of approach of the fluid in the free stream and $\langle \cdot \rangle$ is the Reynolds averaging symbol. Since the particle does not move, $\bar{\boldsymbol{u}}_{r,i} = \bar{\boldsymbol{u}}_e$, where $\bar{\boldsymbol{u}}_e$ is the (instantaneous) velocity of the fluid in the free stream, which is assumed to be statistically uniform and steady.

To correlate these dimensionless groups, these studies measured the mass or heat transfer coefficient for single particles fixed in statistically steady turbulent flows (according to the Chilton-Colburn analogy, these coefficients are equivalent). Due to the free-stream turbulence, the transfer coefficients are random variables, so the measured values are essentially time-averaged quantities. These studies revealed that the influence of L_i was minimal while that of T_i was significant. Eq. (3.1) was modified to:

$$\langle \mathrm{Sh}_i \rangle = A_1 + A_2 A_T^v \mathrm{Re}_i^p \mathrm{Sc}^q \quad ; \quad \mathrm{Re}_i \equiv |\langle \bar{\boldsymbol{u}}_{r,i} \rangle| d_p / \nu_e \tag{3.3}$$

where p and q retain their values from Eq. (3.1), and A_1, A_2 and v are additional constants. A_1, equal to 0 or 2, indicates whether mass transfer owing to molecular diffusion under zero flow conditions is considered; when $\mathrm{Re}_i \gg 1$, this is negligible. A_T depends on Re_i and T_i (see Table 2); even if both are related to $|\langle \bar{\boldsymbol{u}}_{r,i} \rangle|$, these are independent parameters. To decouple them, in experiments one usually fixes the value of Re_i and varies that of T_i by generating the turbulence with a grid upstream of the particle and varying the distance between the grid and the particle.

Table 2 presents several models developed with this approach; these differ in the values of the constants and in the expression for A_T, with some models having a specified validity range. By comparing Eqs. (3.1) and (3.3), we note that free-stream turbulence modifies only the exponent of Re_i, while the exponent of Sc remains unchanged. As shown in the following sections, this finding is consistent with the boundary layer theory but differs from the models derived from penetration theory.

Boundary layer theory

The mass transfer coefficient can be derived using Fick's law, which requires the concentration gradient at the fluid-solid interface. This can be obtained by solving the boundary layer equations [8]. When free-stream turbulence is present, eddies from the fluid bulk penetrate the velocity and concentration boundary layers – provided that the Reynolds and Peclet numbers are large – leading to fluctuations in these regions [20,21]. Because of this unsteadiness, solving the boundary layer equations directly is complex, but doing so is unnecessary, because only the Reynolds-average value of the mass transfer coefficient is usually of interest, and this can be obtained by solving the Reynolds-averaged balance equations. The averaging process simplifies the analysis but introduces additional terms associated with fluctuations, such as the turbulent stress tensor in the averaged linear momentum balance equation and the turbulent dispersion term in the averaged mass balance equation for the solute. These are often modeled using a turbulent diffusivity $\mathscr{D}_t$ (assumed to be the same for momentum and mass), which depends on T_i. With this approach, Ruckenstein [46] and Smith and Kuethe [20] developed correlations for the Nusselt number (equivalent to Sh for mass transfer problems) for flat plates and cylinders, respectively, but no such correlation was established for spheres. Nonetheless, these results allow examining the effect of free-stream turbulence on mass transfer. The results confirm that free-stream turbulence introduces a dependence of Sh on T_i and alters the exponent of Re_i. Conversely, the exponent of Sc remains equal to 1/3, since for liquids the Peclet number is much larger than the Reynolds number, so that the concentration boundary layer is far thinner than the velocity boundary layer, and within the former the velocity profile is essentially linear [8]. These conclusions are consistent with those from the dimensional analysis method.

Penetration theory

To account for free-stream turbulence, several studies have adopted the penetration theory [9,10,27,28,30,47]; this assumes that the solid–liquid interface is made up of a variety of small liquid elements that are continuously brought up to the interface from the bulk of the liquid and vice versa by the motion of the liquid phase. Each liquid element stays at the interface for a time τ_e, known as exposure time. While it is there, each liquid element is assumed to be stagnant, so that mass is transferred within the liquid element solely by unsteady molecular diffusion in the direction perpendicular to the interface [48]. This theory yields the following expression for the mean mass transfer coefficient of a single liquid element over its exposure period:

$$k_\tau = 2\sqrt{\mathscr{D}/\pi\tau_e} \tag{3.4}$$

Following this theory, Kuboi et al. [10] developed correlations for particles with size much larger than the Kolmogorov length scale η. Two exposure time distributions were adopted: a constant one given by $1/\Lambda$, and a randomly distributed one given by $(1/\Lambda)\exp(-\tau_e/\Lambda)$, where Λ is the average exposure time of the liquid elements, taken to be equal to $d_p/u_{r,i}$. With these distributions and Eq. (3.4), one can derive two correlations for the Sherwood number; these are given by:

$$\langle \mathrm{Sh}_i \rangle = 2 + C_c (\mathrm{Re}_i \mathrm{Sc})^{1/2} \quad \text{for} \quad d_p \gg \eta \quad ; \quad \mathrm{Re}_i \equiv u_{r,i} d_p / \nu_e \quad ; \quad u_{r,i} \equiv \sqrt{\langle (\bar{\boldsymbol{u}}_e - \bar{\boldsymbol{u}}_{p,i})^2 \rangle} \tag{3.5}$$

Table 2
Models for mass (or heat) transfer to a fixed particle in a fluid with free-stream turbulence.

Reference	A_1	A_2	A_T	v	Validity range
Yuge [22]	2	0.387	$\mathrm{Re}_i\,\mathrm{T}_i$	0.085	$\mathrm{Re}_i\,\mathrm{T}_i < 7000$
Galloway and Sage [23]	2	1	$0.439 + 1.133813 d_p^{1/2} + 0.234\mathrm{T}_i\,(\mathrm{T}_i + 0.045)\mathrm{Re}_i^{1/2}$	1	$0.01 < \mathrm{T}_i < 0.15$; $2 < \mathrm{Re}_i < 1.33 \cdot 10^6$
Lavender and Pei [21]	2	0.933	$\mathrm{Re}_i\,\mathrm{T}_i$	0.035	$\mathrm{Re}_i\,\mathrm{T}_i < 1000$
	0	0.215	$\mathrm{Re}_i\,\mathrm{T}_i$	0.25	$\mathrm{Re}_i\,\mathrm{T}_i > 1000$
Gostkowski and Costello [24]	0	1.431	$\mathrm{Re}_i\,\mathrm{T}_i$	0.0214	$\mathrm{Re}_i\,\mathrm{T}_i < 7000$
	0	1.287	$\mathrm{Re}_i\,\mathrm{T}_i$	0.2838	$\mathrm{Re}_i\,\mathrm{T}_i > 7000$
Sandoval-Robles et al. [25]	0	0.549	$\mathrm{Re}_i\,\mathrm{T}_i$	0.066	$12 < \mathrm{Re}_i\,\mathrm{T}_i < 600$
Yearling [26]	2	0.52	$1 + 0.07\mathrm{T}_i^{0.843}$	1	$0 < \mathrm{T}_i < 0.11$

For the model by Galloway and Sage [23], the constant in the second term of the expression for A_T has been modified from 0.1807 $\mathrm{in}^{-1/2}$ to 1.133813 $\mathrm{m}^{-1/2}$, because in the original study d_p was expressed in inches while in this study it is expressed in meters.

where $\bar{\boldsymbol{u}}_{p,i}$ is the instantaneous velocity of particle i. For the constant distribution $C_c = 2/\sqrt{\pi}$ (Kuboi et al. incorrectly reported this as $1/\sqrt{\pi}$), while for the other $C_c = 1$. On the right of the equation, the constant 2 was added to account for the case where the slip velocity is zero.

Armenante and Kirwan [30] extended the unsteady-state theory to particles with size far smaller than the Kolmogorov eddy length scale η, assuming that mass transfer occurs while the particles are entrapped in the Kolmogorov eddies, with the exposure time taken to be the Kolmogorov time scale $\Lambda = (\varepsilon/\nu_e)^{-1/2}$, where ε is the Kolmogorov eddy dissipation rate of the surrounding fluid. Using a constant exposure time distribution and Eq. (3.4), they derived the following correlation:

$$\langle \mathrm{Sh}_i \rangle = 2 + C_c \mathrm{Re}_\varepsilon^{3/4} \mathrm{Sc}^{1/2} \quad \text{for} \quad d_p \ll \eta \quad ; \quad \mathrm{Re}_\varepsilon \equiv \varepsilon^{1/3} d_p^{4/3}/\nu_e \tag{3.6}$$

where $C_c = 2/\sqrt{\pi}$ (Armenante and Kirwan reported $C_c = 1/\pi$, but we believe that this is incorrect, because it is inconsistent with Eq. (3.4)).

In Eqs. (3.5) and (3.6), the exponent of the Schmidt number (1/2) differs from that in the Frossling correlation (1/3). This is because the penetration theory essentially assumes that the velocity profile close to the interface between the two phases is uniform; this assumption is accurate for gas–liquid interfaces (since in the liquid, the shear stress is vanishingly small) but not for solid–liquid interfaces, where close to the interface the velocity profile should be taken to be linear. This more realistic assumption results in the exponent of 1/3 featuring in the Frossling correlation. For details, we refer to Bird et al. [8].

3.1.3. Kolmogorov theory

The Kolmogorov theory has also been used to model mass transfer in turbulent systems. In this approach, the correlation shown in Eq. (3.1) is generally used, but the particle Reynolds number is modified by replacing $u_{r,i}$ with the root mean square of the relative velocity between two points in a turbulent flow, defined as:

$$u' \equiv \sqrt{\langle (\bar{\boldsymbol{u}}_{e,1} - \bar{\boldsymbol{u}}_{e,2})^2 \rangle} \tag{3.7}$$

where $\bar{\boldsymbol{u}}_{e,1}$ and $\bar{\boldsymbol{u}}_{e,2}$ are the instantaneous velocities of the fluid at the two points [30–34]. When the distance d between the points is smaller than η, viscous dissipation is important, and it is:

$$u' = (\varepsilon/\nu_e)^{1/2} d \quad \text{for} \quad d \ll \eta \tag{3.8}$$

For distances larger than η, viscous dissipation is unimportant, and u' depends only on ε. Then, dimensional analysis yields:

$$u' = (\varepsilon d)^{1/3}, \quad \text{for} \quad \eta \ll d \ll L \tag{3.9}$$

where L is the characteristic length of the mean flow. In liquid-particle suspensions, d is usually replaced by the particle diameter d_p. This yields:

$$\mathrm{Re}_i \equiv u' d_p/\nu_e = \begin{cases} \varepsilon^{1/2} d_p^2/\nu_e^{3/2} = \mathrm{Re}_\varepsilon^{3/2} & ; \quad d_p \ll \eta \\ \varepsilon^{1/3} d_p^{4/3}/\nu_e = \mathrm{Re}_\varepsilon & ; \quad \eta \ll d_p \ll L \end{cases} \tag{3.10}$$

As we see, Re_i relates to Re_ε (defined in Eq. (3.6)), which is a function of ε. However, the substitution of d by d_p lacks a strong theoretical basis [32].

3.2. Mass transfer coefficient for agitated vessels

3.2.1. Steady-state theory

Some studies have used the steady-state theory to obtain the mass transfer coefficients of individual particles in agitated vessels, using Eq. (3.1) and neglecting the contribution of free-stream turbulence. In this approach, a key point is how to determine the slip velocity $u_{r,i}$.

In agitated vessels, the flow is globally inhomogeneous; hence, particles in different regions of the vessel experience different slip velocities and mass transfer coefficients. To account for this, Hartmann et al. [11] and Hormann et al. [12] used the DPM method, where particle motions are solved using Newton's second law for rigid bodies, with the velocity of each particle calculated, while the equations of motion for the fluid are (locally) volume-averaged and the volume-averaged fluid velocity field, denoted as $\boldsymbol{u}_e$, is calculated. In this framework, the authors defined $u_{r,i}$ as follows:

$$u_{r,i} \equiv |\boldsymbol{u}_e - \bar{\boldsymbol{u}}_{p,i}| \tag{3.11}$$

where $\bar{\boldsymbol{u}}_{p,i}$ denotes the velocity of particle i. Using the calculated slip velocity values in the correlation given by Eq. (3.1), the mass transfer coefficient for each particle was calculated. Subsequently, the mass transfer rate for particle i was obtained using the equation:

$$\frac{dM_{s,i}}{dt} \equiv -k_i A_i (C_s - C) \tag{3.12}$$

Here, $M_{s,i}$ and A_i denote the mass and surface area of particle i, respectively, while C is the locally averaged solute concentration, found by solving the mass balance equation for the solute. Summing the mass transfer rates for all the particles and using the definition of the globally averaged mass transfer coefficient (Eq. (2.1)), one may calculate the latter, provided a characteristic value of $\overline{C}$ is specified. With sufficient data, obtained numerically with the procedure just discussed, one could derive correlations for the globally averaged mass transfer coefficient, but these studies did not explore this. Additionally, the DPM method is computationally demanding and applicable solely for small particle numbers. We should also note that agitated vessels often contain dense suspensions; in these systems, neighboring particles affect the mass transfer for a specific one, making correlations for isolated particles potentially unreliable [16–19].

An alternative approach to determining $u_{r,i}$ is employing the Tchen equation, an equation of motion for small spherical particles in turbulent flow [15]; for a given fluctuating fluid velocity $\bar{\boldsymbol{u}}_e$, solving the Tchen equation yields the instantaneous particle velocity $\bar{\boldsymbol{u}}_{p,i}$. Then, $u_{r,i}$ is calculated via Eq. (3.5)C [9,10,29]. Notice that the Tchen equation is based on several assumptions. It assumes a statistically steady turbulent flow, which is not always present in agitated vessels. It assumes as well that the particle diameter is smaller than the Kolmogorov eddy length

scale – a condition that is not always satisfied; nevertheless, Harriott [9] justified the applicability of the solution of the Tchen equation when $d_p \gg \eta$, which is also supported by Kuboi et al. [10,29]. Finally, the Tchen equation assumes that near the particle the turbulent flow is homogeneous, a condition approximated by the local homogeneity assumption.

With these assumptions, and assuming that particles respond only to eddies larger than their size, Kuboi et al. [10,29] solved the Tchen equation analytically. The solution indicated that the slip velocity depends on the fluctuating fluid velocity $\bar{u}_e$ and on the drag coefficient of the particle in the turbulent flow, which was found to depend on the Kolmogorov eddy dissipation rate ε of the surrounding fluid. Since in agitated vessels the flow is globally inhomogeneous, $\bar{u}_e$ and ε vary spatially, resulting in different values of the slip velocity for different particles. However, instead of accounting for this variability, the authors assumed a constant slip velocity for all the particles, calculated using the fluid velocity measured in a specific sampling point within the vessel and the mean (over the entire vessel) Kolmogorov dissipation rate $\bar{\varepsilon}$. Using this slip velocity in Eq. (3.1), applying either the correlation by Friedlander [14] or that by Frossling [13], the authors calculated the globally averaged mass transfer coefficient. The predictions underestimated the experimental data, with relative percent errors greater than 30%. This was attributed to the deficiency of the steady-state theory, but additional factors may have introduced inaccuracies; for instance, in dense suspensions, particle interactions might affect the relative motions between the fluid and the particles – an effect that is neglected in the Tchen equation. Furthermore, some assumptions (e.g., that a constant slip velocity can be used for all the particles and that correlations for isolated particles can be used) may cause inaccuracies.

3.2.2. Unsteady-state theory

As discussed in Section 3.1.2, several methods have been proposed to account for the effect of free-stream turbulence on mass transfer. However, the correlations derived using the dimensional analysis method hold for isolated particles fixed in turbulent flows, and their applicability to agitated vessels, where both the fluid and the particles are in motion and a large number of particles are involved, has not been investigated. In the case of the boundary layer theory, no correlations are available for spherical particles. Thus, in this section, we only consider the studies employing the penetration theory.

Penetration theory

As shown in Eq. (3.5), applying the correlations developed by Kuboi et al. [10] to calculate the mass transfer coefficient for a particle in agitated vessels requires the slip velocity $u_{r,i}$. As stated for this study in the previous section, the authors assumed a constant slip velocity for all particles. This simplification allows using Eq. (3.5) to obtain the globally averaged coefficient. Their results indicated that the constant exposure time assumption leads to a better fit with their experimental data on liquid-particle mass transfer coefficients. But the limitations associated with determining $u_{r,i}$, discussed in the previous section, still stand. Furthermore, as discussed, the assumption of a uniform velocity profile near the interface – central to penetration theory – is not valid for liquid-particle systems, limiting its theoretical justification.

Armenante and Kirwan [30] also assumed a uniform Sherwood number for all the particles and modified the correlation given by Eq. (3.6), replacing Re_ε with $\mathrm{Re}_{\bar{\varepsilon}}$, to obtain the globally averaged Sherwood number. Because their initial calculation of C_c was inaccurate, the authors subsequently adjusted its value to better fit their experimental data, yet they still did not achieve good agreement. These deviations might stem from the use of $\mathrm{Re}_{\bar{\varepsilon}}$ and the assumptions inherent to the penetration theory.

3.2.3. Kolmogorov theory

Two main approaches have been used to apply the Kolmogorov theory to obtain the mass transfer coefficient in agitated vessels. The first involves calculating the local mass transfer coefficient by evaluating the spatial distribution of ε. To do this, Xie et al. [49] adopted a turbulent multifluid model. However, ε quantifies the microscale dissipation rate of turbulent kinetic energy, which is related to the fluctuations of the fluid point velocity; as discussed by Fox [50], the turbulent multifluid model instead yields the macroscale dissipation rate of turbulent kinetic energy, which is related to the fluctuations of the fluid mean velocity. Therefore, the method by Xie et al. [49] may be inaccurate.

More commonly, similarly to the approach of Kuboi et al. [10], studies using the Kolmogorov theory adopt a simplified approach in which ε in Eq. (3.10) is replaced by $\bar{\varepsilon}$ and $\mathrm{Re}_{\bar{\varepsilon}}$ is employed in correlations of the same form as Eq. (3.1) to calculate the globally averaged mass transfer coefficient. Following this theory, Armenante and Kirwan [30] developed a correlation for particles with $d_p \ll \eta$. For these, $\mathrm{Re}_i = \varepsilon^{1/2} d_p^2 / \nu_e^{3/2} = (d_p/\eta)^2 \ll 1$, since $\eta = \nu_e^{3/4}/\varepsilon^{1/4}$. Consequently, the authors adopted the correlation for creeping flows by Friedlander [14], obtaining:

$$\langle \overline{\mathrm{Sh}} \rangle = 2 + 0.991 \mathrm{Re}_{\bar{\varepsilon}}^{1/2} \mathrm{Sc}^{1/3} \quad \text{for} \quad d_p \ll \eta \tag{3.13}$$

where $\overline{\mathrm{Sh}}$ is the globally averaged Sherwood number. To better fit their experimental data, both the constant 0.991 and the exponent of $\mathrm{Re}_{\bar{\varepsilon}}$ were then modified to 0.52.

For particles with $d_p \gg \eta$, Calderbank and Moo-Young [31] neglected in Eq. (3.1) the constant 2, set q to 1/3 (in line with the boundary layer theory) and estimated C_c and p experimentally. The resulting correlation is given by:

$$\langle \overline{\mathrm{Sh}} \rangle = 0.13 \mathrm{Re}_{\bar{\varepsilon}}^{3/4} \mathrm{Sc}^{1/3} \quad \text{for} \quad d_p \gg \eta \tag{3.14}$$

By analyzing experimental data, Levins and Glastonbury [32] observed that, in addition to $\mathrm{Re}_{\bar{\varepsilon}}$ and Sc, $\langle \overline{\mathrm{Sh}} \rangle$ also depends on the fluid-particle density ratio and the impeller-to-vessel diameter ratio, but did not propose a correlation. Bong et al. [34] investigated the effect of the initial solid volume fraction when $d_p \gg \eta$, set the values of p and q the same as those in the correlation by Frossling [13], while modeled C_c as a function of $\mathrm{Re}_{\bar{\varepsilon}}$, obtaining the following relation:

$$C_c = -b_1 \mathrm{Re}_{\bar{\varepsilon}}^{1/2} + b_2 - b_3 \mathrm{Re}_{\bar{\varepsilon}}^{-1/2} \tag{3.15}$$

Since the initial solid volume fraction was found to affect $\bar{\varepsilon}$, its effect on mass transfer was considered. Here, b_1, b_2 and b_3 are constants; their values were found to change when experimental conditions (e.g., the vessel size) vary, limiting the applicability of the resulting correlation.

3.2.4. Dimensional analysis method

In this method, one first identifies the parameters characterizing the mass transfer process between the liquid and the particles in an agitated vessel, and then applies the Buckingham theorem to determine the relevant dimensionless groups. Finally, these groups are correlated using experimental data.

Hixson and Baum [1] identified as key parameters the impeller rotation speed, the vessel diameter, the liquid density and viscosity, and the solute diffusivity, denoted as N, d_V, ρ_e, μ_e and $\mathscr{D}$, respectively. These resulted in the following dimensionless numbers:

$$\overline{\mathrm{Sh}}_V \equiv \bar{k} d_V / \mathscr{D} \quad ; \quad \mathrm{Re}_V \equiv N d_V^2 / \nu_e \quad ; \quad \mathrm{Sc} \equiv \nu_e / \mathscr{D} \tag{3.16}$$

Here, the Sherwood and Reynolds numbers are characterized by the vessel diameter d_V. To fit experimental data from their study and that of Hixson and Wilkens [35], the authors used the correlation:

$$\overline{\mathrm{Sh}}_V = C_c \mathrm{Re}_V^p \mathrm{Sc}^q \tag{3.17}$$

Here, C_c, p and q are constants. Due to the narrow range of Sc in the data, Hixson and Baum [1] directly set q to 1/2, following penetration theory. Then, they obtained C_c and p from data analysis, finding $C_c = 0.16$ and $p = 0.62$ for $\mathrm{Re}_V > 6.7 \cdot 10^4$, and $C_c = 2.7 \cdot 10^{-5}$ and $p = 1.4$ for

lower values of Re_V. Note that the data used by Hixson and Baum refer to vessels without baffles, while for all the other studies considered in our article, the data refer to baffled vessels. By reanalyzing the data used in Hixson and Baum [1] and Marangozis and Johnson [5] found that taking $q = 1/3$, consistent with the boundary layer theory, and C_c and p to be constant over the entire Re_V range provides better agreement with the experimental data. However, they did not calculate the values of C_c and p. Other researchers used Eq. (3.17), with $q = 1/2$, to correlate their data; Humphrey and Van Ness [2] found $C_c = 0.13$ and $p = 0.58$ for propellers and $C_c = 0.0032$ and $p = 0.87$ for turbines, while for the latter Barker and Treybal [3] found $C_c = 0.02$ and $p = 0.833$.

In the dimensional analysis of the system, Sykes and Gomezplata [6] included as additional parameters the impeller diameter d_I and the initial particle diameter $d_{p,0}$. However, in the correlation they used, they did not include two additional dimensionless numbers, modifying Eq. (3.17) to:

$$\overline{\mathrm{Sh}} = 2 + C_c \mathrm{Re}_I^p \mathrm{Sc}^q \tag{3.18}$$

with:

$$\overline{\mathrm{Sh}} \equiv \overline{k} d_{p,0}/\mathscr{D} \quad ; \quad \mathrm{Re}_I \equiv N d_I^2/\nu_e \tag{3.19}$$

As we see, the Sherwood number features the initial particle diameter, while the Reynolds number features the impeller diameter. For a given geometry, the ratio between d_I and d_V is specified, making Re_I equivalent to Re_V. The authors estimated the values of the constants in Eq. (3.18) via data analysis, finding that $q = 1/2$ provided a better fit, with $C_c = 0.109$ and $p = 0.34$.

Nagata et al. [4] included the effects of gravity and the density difference between the liquid and the particles, proposing the following correlation:

$$\overline{\mathrm{Sh}}_V = C_c \mathrm{Re}_V^p \mathrm{Sc}^q \left(\frac{\mathscr{D}^2}{g d_V^3}\right)^a \left(\frac{d_{p,0}}{d_V}\right)^b \left(\frac{\rho_s - \rho_e}{\rho_e}\right)^c \tag{3.20}$$

where g is the gravitational acceleration. Via data analysis, they found C_c, a, b and c to be equal to $3.6 \cdot 10^{12}$, 0.627, 3.08 and -2.82, respectively, while p and q resulted to be functions of all the dimensionless groups featuring on the right-hand side of Eq. (3.20) except the Reynolds number.

Boon-Long et al. [7] included in the analysis the effect of the initial solid volume fraction $\overline{\alpha}_{s,0}$, but due to the limited range in the available data about the density difference between the liquid and the particles, they excluded this parameter, proposing this correlation:

$$\overline{\mathrm{Sh}} = C_c \mathrm{Re}_d^p \mathrm{Sc}^q \mathrm{Ga}^a \left(\frac{d_{p,0}}{d_V}\right)^b \psi^c \tag{3.21}$$

Here, Re_d is a Reynolds number related to the particle diameter, Ga is the Galilei number and ψ relates to the initial solid volume fraction, defined as:

$$\mathrm{Re}_d \equiv \frac{2\pi^2 N d_V d_{p,0}}{\nu_e} \quad ; \quad \mathrm{Ga} \equiv \frac{g d_{p,0}^3}{\nu_e^2} \quad ; \quad \psi \equiv \frac{M_{s,0}}{\rho_e d_{p,0}^3} \tag{3.22}$$

Through data analysis, the authors found $C_c = 0.046$, $p = 0.283$, $q = 0.461$, $a = 0.173$, $b = -0.019$ and $c = -0.011$, respectively.

As shown, studies based on the dimensional analysis method may overlook some dimensionless groups. While Boon-Long et al. [7] did consider the most influential factors, the effects of some groups could not be studied owing to limitations in experimental data. Furthermore, as noted by Bird et al. [8], this method requires geometric similarity; therefore, correlations derived for an agitated vessel with a specific geometry are inapplicable if the geometry changes – a problem often encountered in industrial processes.

4. Methodology

In Section 3.2, we reviewed the main methods for calculating the globally averaged mass transfer coefficient in agitated vessels, all of which exhibit certain limitations. To address these limitations, we have developed a new method for calculating this coefficient. In Section 4.1, we discuss the relationship between the globally averaged and the locally volume-averaged mass transfer coefficients, considering the effects of neighboring particles and free-stream turbulence. To determine the distribution of the local mass transfer coefficient, the profiles of fluid dynamic variables (such as the velocities and volume fractions of the liquid and solid phases) are required; these are calculated via a turbulent multifluid model, whose balance and constitutive equations are presented in Section 4.2.

4.1. Derivation of the coefficient

4.1.1. Relationship between the globally and locally averaged coefficients

In an agitated vessel, the global mass transfer rate between the liquid and the particles, denoted as dM_V/dt, is obtained by integrating the local mass transfer rate per unit volume, denoted as dM/dt, over the volume V_V occupied by the suspension:

$$\frac{dM_V}{dt} = \int_{V_V} \frac{dM}{dt} dV \tag{4.1}$$

dM/dt can be expressed in terms of the locally volume-averaged mass transfer coefficient k_L via the below equation, where A_L denotes the particle surface area per unit volume:

$$\frac{dM}{dt} \equiv k_L A_L (C_s - C) \quad ; \quad A_L \equiv 6\alpha_s/d_p \tag{4.2}$$

Following the discussion after Eq. (2.2), a constant particle diameter is assumed for all particles. Furthermore, although the fluid dynamics in the vessel is inhomogeneous, the suspension in a small local region can be assumed to be homogeneous, with an associated value of k_L.

Employing Eqs. (2.1) and (4.1), a relationship between the global and local mass transfer coefficients can be established; this is given by:

$$\overline{k} = \frac{1}{\overline{\alpha}_{s,0} V_V} \int_{V_V} \left(\frac{C_s - C}{C_s - \overline{C}}\right) \alpha_s k_L dV \quad \Rightarrow \quad \overline{\mathrm{Sh}} = \frac{1}{\overline{\alpha}_{s,0} V_V} \times \int_{V_V} \left(\frac{C_s - C}{C_s - \overline{C}}\right) \alpha_s \mathrm{Sh}_L dV \tag{4.3}$$

where Sh_L is the local Sherwood number. We now assume that the solute concentration is much smaller than the saturation concentration, simplifying Eq. (4.3)B to:

$$\overline{\mathrm{Sh}} = \frac{1}{\overline{\alpha}_{s,0} V_V} \int_{V_V} \alpha_s \mathrm{Sh}_L dV \tag{4.4}$$

This simplification permits neglecting the solute concentration, so that the solute mass balance equation does not have to be solved; this reduces the complexity of the model significantly (but of course, if this assumption cannot be applied, the model can be easily generalized).

4.1.2. Effect of particle interactions and free-stream turbulence

To account for the effect of particle interactions on the mass transfer of an individual particle, we obtain Sh_L via the correlation of Wang et al. [19]:

$$\mathrm{Sh}_L = \frac{B}{2} \alpha_e^{-2(m-1)/3} \left[0.63 \mathrm{Re}_i + 4.8 \mathrm{Re}_i^{1/2} \alpha_e^{(m-1)/2}\right]^{2/3} \mathrm{Sc}^{1/3} \quad ; \quad \mathrm{Pe}_i \gg 1 \tag{4.5}$$

where α_e is the liquid-phase volume fraction, while Re_i and Pe_i are the particle Reynolds number and Peclet number, respectively; these numbers are defined as:

$$\mathrm{Re}_i \equiv |\boldsymbol{u}_e - \boldsymbol{u}_s| d_p/\nu_e \quad ; \quad \mathrm{Pe}_i \equiv |\boldsymbol{u}_e - \boldsymbol{u}_s| d_p/\mathscr{D} \tag{4.6}$$

where $\boldsymbol{u}_e$ and $\boldsymbol{u}_s$ are the locally volume-averaged velocities of the liquid and solid phases, respectively. B is a constant, whose value depends on

the range of Re_i, while m is given by:

$$m = \frac{4.8 + 2.4 \cdot 0.175\mathrm{Re}_t^{3/4}}{1 + 0.175\mathrm{Re}_t^{3/4}} \quad ; \quad \mathrm{Re}_t \equiv u_t d_p/\nu_e = \alpha_e^{-(m-1)}\mathrm{Re}_i \tag{4.7}$$

where Re_t is the Reynolds number based on the particle terminal velocity u_t. Eq. (4.5) holds only for $\mathrm{Pe}_i \gg 1$, as it is derived from the concentration boundary layer theory; when this condition is not met, a term for mass transfer under zero flow conditions should be included; for details, see Wang et al. [19].

The above correlation was derived under the condition that there is no free-stream turbulence. However, in agitated vessels turbulence often exists, so Eq. (4.5) must be modified to account for its effect. To do this, we Reynolds average Eq. (4.4). The result and the subsequent passages involve Reynolds averages, fluid averages and solid averages. For a given locally volume-averaged (or Eulerian) variable ζ, these averages are denoted as $\langle\zeta\rangle$, $\langle\zeta\rangle_E$ and $\langle\zeta\rangle_S$, respectively, and the corresponding fluctuating quantities are denoted by ζ', ζ'' and ζ''', respectively. The fluid and solid averages are related to the Reynolds averages as follows:

$$\langle\zeta\rangle_E \equiv \langle\alpha_e\zeta\rangle/\langle\alpha_e\rangle \quad ; \quad \langle\zeta\rangle_S \equiv \langle\alpha_s\zeta\rangle/\langle\alpha_s\rangle \tag{4.8}$$

Using these variables, we obtain:

$$\langle\overline{\mathrm{Sh}}\rangle = \frac{1}{\overline{\alpha}_{s,0}V_V}\int_{V_V}\langle\alpha_s\mathrm{Sh}_L\rangle dV = \frac{1}{\overline{\alpha}_{s,0}V_V}\int_{V_V}\langle\alpha_s\rangle\langle\mathrm{Sh}_L\rangle_S dV \tag{4.9}$$

In calculating $\langle\mathrm{Sh}_L\rangle_S$, to account for the effect of free-stream turbulence, we follow the method employed to develop Eq. (3.3), the correlation for a fixed particle in a turbulent flow. As the systems of interest have large Peclet number, the constant A_1 accounting for mass transfer under zero flow conditions can be neglected, so that Eq. (3.3) can be simplified to:

$$\langle\mathrm{Sh}_i\rangle = A_2[A_T(\mathrm{Re}_i, \mathrm{T}_i)]^v\mathrm{Re}_i^p\mathrm{Sc}^q = A_2[A_T(\mathrm{Re}_i, \mathrm{T}_i)]^v[\mathrm{Sh}_i(\mathrm{Re}_i, \mathrm{Sc})/C_c] \tag{4.10}$$

where Sh_i is calculated via Eq. (3.1)A, but with the constant 2 neglected. In Eq. (4.10), we have emphasized that A_T is a function of the particle Reynolds number Re_i and of the turbulent intensity T_i (but in some models, it depends only on T_i), while Sh_i is a function of the Schmidt number and of Re_i. The latter is defined in terms of the Reynolds-averaged slip velocity between the phases (Eq. (3.3)B), while the turbulent intensity depends on this velocity and its fluctuations (Eq. (3.2)).

In analogy, in agitated vessels where many particles are involved, and both the fluid and the particles are in motion, $\langle\mathrm{Sh}_L\rangle$ is calculated with the following equation:

$$\langle\mathrm{Sh}_L\rangle = A_2[A_T(\mathrm{Re}_i, \mathrm{T}_i)]^v[\mathrm{Sh}_L(\langle\alpha_e\rangle, \mathrm{Re}_i, \mathrm{Sc})/\kappa] \tag{4.11}$$

where κ is a constant. Nevertheless, as shown in Eq. (4.9), to calculate $\langle\overline{\mathrm{Sh}}\rangle$, $\langle\mathrm{Sh}_L\rangle_S$ is required. To relate it to $\langle\mathrm{Sh}_L\rangle$, this expression, derived by Fox [50], is used:

$$\langle\zeta\rangle_S = \langle\zeta\rangle + \langle\alpha_s'\zeta\rangle/\langle\alpha_s\rangle \tag{4.12}$$

which yields:

$$\langle\mathrm{Sh}_L\rangle_S = \langle\mathrm{Sh}_L\rangle + \langle\alpha_s'\mathrm{Sh}_L\rangle/\langle\alpha_s\rangle \tag{4.13}$$

In this equation, $\langle\alpha_s'\mathrm{Sh}_L\rangle$ is neglected for the lack of a good closure; this is analogous to what Fox and other researchers have done, for instance, for fluid-velocity triple correlations. With this approximation, $\langle\mathrm{Sh}_L\rangle_S$ is equal to $\langle\mathrm{Sh}_L\rangle$ and can thus be calculated via Eq. (4.11).

Similarly to Eq. (4.10), in Eq. (4.11) Sh_L depends on Re_i and Sc, while A_T is a function of Re_i and T_i. Re_i is calculated using the Reynolds-averaged slip velocity $\langle\boldsymbol{u}_e\rangle - \langle\boldsymbol{u}_s\rangle$, while T_i depends not only on the latter but also on the slip-velocity fluctuations $\boldsymbol{u}_e' - \boldsymbol{u}_s'$. However, as we shall see in Section 4.2, the fluid dynamic model yields (only) phase-averaged velocities and their relevant fluctuations; hence, in the definitions of both Re_i and T_i, the Reynolds-averaged variables must be expressed in terms of their phase-averaged counterparts.

In Eq. (4.11), Re_i is defined as:

$$\mathrm{Re}_i \equiv |\langle\boldsymbol{u}_e\rangle - \langle\boldsymbol{u}_s\rangle|d_p/\nu_e \tag{4.14}$$

Here, $\langle\boldsymbol{u}_e\rangle - \langle\boldsymbol{u}_s\rangle$ must be expressed in terms of $\langle\boldsymbol{u}_e\rangle_E - \langle\boldsymbol{u}_s\rangle_S$. To this end, Eq. (4.12) and the following relationship, derived by Fox [50], are employed:

$$\langle\zeta\rangle_E = \langle\zeta\rangle - \langle\alpha_s'\zeta\rangle/\langle\alpha_e\rangle \tag{4.15}$$

This yields:

$$\langle\boldsymbol{u}_e\rangle = \langle\boldsymbol{u}_e\rangle_E + \langle\alpha_s'\boldsymbol{u}_e\rangle/\langle\alpha_e\rangle \quad ; \quad \langle\boldsymbol{u}_s\rangle = \langle\boldsymbol{u}_s\rangle_S - \langle\alpha_s'\boldsymbol{u}_s\rangle/\langle\alpha_s\rangle \tag{4.16}$$

whence:

$$\langle\boldsymbol{u}_e\rangle - \langle\boldsymbol{u}_s\rangle = \langle\boldsymbol{u}_e\rangle_E - \langle\boldsymbol{u}_s\rangle_S + \left(\frac{\langle\alpha_s'\boldsymbol{u}_e\rangle}{\langle\alpha_e\rangle} + \frac{\langle\alpha_s'\boldsymbol{u}_s\rangle}{\langle\alpha_s\rangle}\right) \tag{4.17}$$

Next, we relate $\langle\alpha_s'\boldsymbol{u}_e\rangle$ and $\langle\alpha_s'\boldsymbol{u}_s\rangle$. These are equal to $\langle\alpha_s'\boldsymbol{u}_e''\rangle$ and $\langle\alpha_s'\boldsymbol{u}_s'''\rangle$, respectively. According to the transport equation for the phasic turbulent kinetic energies reported in Fox [50] (see pages 382, 385, 397, 418 and 420), it is:

$$\langle\alpha_s'\boldsymbol{u}_e''\rangle - \langle\alpha_s'\boldsymbol{u}_s'''\rangle = -C_p\langle\alpha_e\rangle(\langle\boldsymbol{u}_e\rangle_E - \langle\boldsymbol{u}_s\rangle_S) \tag{4.18}$$

In Wang and Mazzei [51], who applied the Fox model to simulate liquid-particle flows in agitated vessels, it was found that $C_p = 0$ provides good predictions, so that $\langle\alpha_s'\boldsymbol{u}_e''\rangle$ and $\langle\alpha_s'\boldsymbol{u}_s'''\rangle$ are equal. Using this relation in Eq. (4.17), we then obtain:

$$\langle\boldsymbol{u}_e\rangle - \langle\boldsymbol{u}_s\rangle = \langle\boldsymbol{u}_e\rangle_E - \langle\boldsymbol{u}_s\rangle_S + \boldsymbol{u}_{dr} \quad ; \quad \boldsymbol{u}_{dr} \equiv \frac{\langle\alpha_s'\boldsymbol{u}_e''\rangle}{\langle\alpha_e\rangle\langle\alpha_s\rangle} \tag{4.19}$$

Here, $\boldsymbol{u}_{dr}$ is referred to as drift velocity (see Section 4.2 for further details); its presence does not causes any problems, because this velocity is calculated by the fluid dynamic model. With this last equation, Eq. (4.14) can be expressed as:

$$\mathrm{Re}_i = |\langle\boldsymbol{u}_e\rangle_E - \langle\boldsymbol{u}_s\rangle_S + \boldsymbol{u}_{dr}|d_p/\nu_e \tag{4.20}$$

which is now in closed form and can be used to calculate Re_i in Eq. (4.11).

In Eq. (4.11), T_i is defined as:

$$\mathrm{T}_i \equiv \frac{1}{|\langle\boldsymbol{u}_e\rangle - \langle\boldsymbol{u}_s\rangle|}\sqrt{\frac{\langle(\boldsymbol{u}_e' - \boldsymbol{u}_s')^2\rangle}{3}} \tag{4.21}$$

This definition is inconvenient, because it is in terms of $\boldsymbol{u}_e'$ and $\boldsymbol{u}_s'$, whereas, as discussed in Section 4.2, the fluid dynamic model yields properties related to $\boldsymbol{u}_e''$ and $\boldsymbol{u}_s'''$. To overcome this issue, we use the following transformations:

$$\begin{aligned}\boldsymbol{u}_e' &= \boldsymbol{u}_e - \langle\boldsymbol{u}_e\rangle = \boldsymbol{u}_e - \langle\boldsymbol{u}_e\rangle_E - \langle\alpha_s'\boldsymbol{u}_e\rangle/\langle\alpha_e\rangle = \boldsymbol{u}_e'' - \langle\alpha_s'\boldsymbol{u}_e\rangle/\langle\alpha_e\rangle\\ \boldsymbol{u}_s' &= \boldsymbol{u}_s - \langle\boldsymbol{u}_s\rangle = \boldsymbol{u}_s - \langle\boldsymbol{u}_s\rangle_S + \langle\alpha_s'\boldsymbol{u}_s\rangle/\langle\alpha_s\rangle = \boldsymbol{u}_s''' + \langle\alpha_s'\boldsymbol{u}_s\rangle/\langle\alpha_s\rangle\end{aligned} \tag{4.22}$$

where Eqs. (4.12) and (4.15) have been used. This yields:

$$\boldsymbol{u}_e' - \boldsymbol{u}_s' = \boldsymbol{u}_e'' - \boldsymbol{u}_s''' - \left(\frac{\langle\alpha_s'\boldsymbol{u}_e\rangle}{\langle\alpha_e\rangle} + \frac{\langle\alpha_s'\boldsymbol{u}_s\rangle}{\langle\alpha_s\rangle}\right) = \boldsymbol{u}_e'' - \boldsymbol{u}_s''' - \boldsymbol{u}_{dr} \tag{4.23}$$

Accordingly, we have:

$$\begin{aligned}&\langle(\boldsymbol{u}_e' - \boldsymbol{u}_s')^2\rangle = \langle(\boldsymbol{u}_e'' - \boldsymbol{u}_s''' - \boldsymbol{u}_{dr})^2\rangle\\ &= \langle\boldsymbol{u}_e''\cdot\boldsymbol{u}_e''\rangle + \langle\boldsymbol{u}_s'''\cdot\boldsymbol{u}_s'''\rangle - 2\langle\boldsymbol{u}_e''\cdot\boldsymbol{u}_s'''\rangle - 2\langle(\boldsymbol{u}_e'' - \boldsymbol{u}_s''')\cdot\boldsymbol{u}_{dr}\rangle + \langle\boldsymbol{u}_{dr}\cdot\boldsymbol{u}_{dr}\rangle\end{aligned} \tag{4.24}$$

As we see from Eq. (4.19)B, $\boldsymbol{u}_{dr}$ is a function of (ensemble) averaged variables – that is, $\boldsymbol{u}_{dr}$ is not a random variable. So, $\langle\boldsymbol{u}_{dr}\rangle = \boldsymbol{u}_{dr}$. Moreover, as reported by Fox [50], it is:

$$\langle\alpha_s'\zeta\rangle = \langle\alpha_s'\zeta''\rangle = \langle\alpha_s'\zeta'''\rangle = \langle\alpha_e\rangle\langle\zeta''\rangle = -\langle\alpha_s\rangle\langle\zeta'''\rangle \tag{4.25}$$

Thus, we have:

$$\langle\boldsymbol{u}_e'' - \boldsymbol{u}_s'''\rangle = \frac{\langle\alpha_s'\boldsymbol{u}_e''\rangle}{\langle\alpha_e\rangle} + \frac{\langle\alpha_s'\boldsymbol{u}_s'''\rangle}{\langle\alpha_s\rangle} = \boldsymbol{u}_{dr} \tag{4.26}$$

Using Eqs. (4.12) and (4.15), the first three terms on the right-hand side of Eq. (4.24) are rewritten as:

$$\langle \boldsymbol{u}_e'' \cdot \boldsymbol{u}_e'' \rangle = \langle \boldsymbol{u}_e'' \cdot \boldsymbol{u}_e'' \rangle_E + \langle \alpha_s' \boldsymbol{u}_e'' \cdot \boldsymbol{u}_e'' \rangle / \langle \alpha_e \rangle \quad ;$$
$$\langle \boldsymbol{u}_s''' \cdot \boldsymbol{u}_s''' \rangle = \langle \boldsymbol{u}_s''' \cdot \boldsymbol{u}_s''' \rangle_S - \langle \alpha_s' \boldsymbol{u}_s''' \cdot \boldsymbol{u}_s''' \rangle / \langle \alpha_s \rangle \quad ;$$
$$\langle \boldsymbol{u}_e'' \cdot \boldsymbol{u}_s''' \rangle = \langle \boldsymbol{u}_e'' \cdot \boldsymbol{u}_s''' \rangle_S - \langle \alpha_s' \boldsymbol{u}_e'' \cdot \boldsymbol{u}_s''' \rangle / \langle \alpha_s \rangle \tag{4.27}$$

Here, the second terms on the right-hand sides of the above relations are neglected for lack of good closures, see page 397 in Fox [50], while the first terms are related to the turbulent kinetic energies of the phases, see pages 378 and 395 in Fox [50], given by:

$$\langle \boldsymbol{u}_e'' \cdot \boldsymbol{u}_e'' \rangle_E = 2k_e \quad ; \quad \langle \boldsymbol{u}_s''' \cdot \boldsymbol{u}_s''' \rangle_S = 2k_s \quad ; \quad \langle \boldsymbol{u}_e'' \cdot \boldsymbol{u}_s''' \rangle_S = 2(k_e k_s)^{1/2} \tag{4.28}$$

Here, k_e and k_s represent the turbulent kinetic energies of the fluid and solid phases, respectively, which can be calculated by the multifluid model presented in Section 4.2. Using these expressions, we have:

$$\langle (\boldsymbol{u}_e' - \boldsymbol{u}_s')^2 \rangle = 2\left(\sqrt{k_e} - \sqrt{k_s}\right)^2 - \boldsymbol{u}_{dr}^2 \tag{4.29}$$

Using this relation and Eq. (4.19)A in Eq. (4.21) yields:

$$\mathrm{T}_i = \frac{1}{|\langle \boldsymbol{u}_e \rangle_E - \langle \boldsymbol{u}_s \rangle_S + \boldsymbol{u}_{dr}|} \sqrt{\frac{2\left(\sqrt{k_e} - \sqrt{k_s}\right)^2 - \boldsymbol{u}_{dr}^2}{3}} \tag{4.30}$$

which is now in closed form and can be used to calculate T_i in Eq. (4.11).

Finally, we must determine the value of the constant κ. To do so, we start from the correlation for isolated particles derived in Wang et al. [19] and then extend the analysis to the case of suspensions. For the case of isolated particles, in the absence of free-stream turbulence, the correlation derived by Wang et al. [19] is given by the following expression:

$$\mathrm{Sh}_i = \frac{B_i}{2}\left(0.63\mathrm{Re}_i + 4.8\mathrm{Re}_i^{1/2}\right)^{2/3}\mathrm{Sc}^{1/3} \quad ; \quad B_i = \begin{cases} 0.682 & \text{for} \quad \mathrm{Re}_i < 0.1 \\ 0.469 & \text{for} \quad \mathrm{Re}_i > 10 \end{cases} \tag{4.31}$$

As we see, this contains different exponents for Re_i. Next, we reformulate it in the form of Eq. (3.1)A, since doing this facilitates the determination of κ.

When $\mathrm{Re}_i \ll 50$, we have $0.63\mathrm{Re}_i \ll 4.8\mathrm{Re}_i^{1/2}$; therefore, the first term in the bracket of Eq. (4.31)A can be neglected, leading to:

$$\left(0.63\mathrm{Re}_i + 4.8\mathrm{Re}_i^{1/2}\right)^{2/3} \approx \left(4.8\mathrm{Re}_i^{1/2}\right)^{2/3} \quad \text{for} \quad \mathrm{Re}_i \ll 50 \tag{4.32}$$

For $\mathrm{Re}_i < 0.1$, this approximation yields a relative error within 3%, giving:

$$\mathrm{Sh}_i = \frac{B_i}{2} 4.8^{2/3}\mathrm{Re}_i^{1/3}\mathrm{Sc}^{1/3} = 1.423 B_i \mathrm{Re}_i^{1/3}\mathrm{Sc}^{1/3} \quad \text{for} \quad \mathrm{Re}_i < 0.1 \tag{4.33}$$

Thus, $\kappa = 1.423 B_i$. Although the value of B_i is not required, as it cancels out in Eq. (4.10), using $B_i = 0.682$ results in $\kappa = 0.97$, which is very close to the constant 0.991 used by Friedlander [14]. Furthermore, the exponent of Re_i is also consistent.

In Eq. (3.1)A, for $\mathrm{Re}_i \gg 1$, the exponent of Re_i used by Frossling [13] is 1/2. Accordingly, in Eq. (4.31), we require that:

$$\left(0.63\mathrm{Re}_i + 4.8\mathrm{Re}_i^{1/2}\right)^{2/3} \sim \mathrm{Re}_i^{1/2} \tag{4.34}$$

This can be equivalently written as:

$$\left(0.63^2\mathrm{Re}_i^2 + 2 \cdot 0.63 \cdot 4.8\mathrm{Re}_i^{3/2} + 4.8^2\mathrm{Re}_i\right)^{1/3} \sim \mathrm{Re}_i^{1/2} \tag{4.35}$$

This condition is met when the term featuring $\mathrm{Re}_i^{3/2}$ on the left-hand side dominates over the other two terms. This occurs for $10 \ll \mathrm{Re}_i \ll 250$. This range is quite small, but for most values of Re_i within this range, the first or the third term in the bracket is comparable to the second term; thus, a good approximation is:

$$\left(0.63^2\mathrm{Re}_i^2 + 2 \cdot 0.63 \cdot 4.8\mathrm{Re}_i^{3/2} + 4.8^2\mathrm{Re}_i\right)^{1/3} \approx (2 \cdot 2 \cdot 0.63 \cdot 4.8)^{1/3}\mathrm{Re}_i^{1/2} \tag{4.36}$$

For $10 < \mathrm{Re}_i < 250$, this approximation results in a relative error within 7%. Examining its applicability for larger values of Re_i, we find that even for Re_i up to 1000, the relative error is within 15%. Thus, Eq. (4.31)A is rewritten as:

$$\mathrm{Sh}_i = \frac{B_i}{2}(2 \cdot 2 \cdot 0.63 \cdot 4.8)^{1/3}\mathrm{Re}_i^{1/2}\mathrm{Sc}^{1/3} = 1.148 B_i \mathrm{Re}_i^{1/2}\mathrm{Sc}^{1/3} \quad \text{for} \quad 10 < \mathrm{Re}_i < 1000 \tag{4.37}$$

In this case, $\kappa = 1.148 B_i$. Taking $B_i = 0.469$ yields $\kappa = 0.538$, which is very close to the constant 0.552 by Frossling [13]. The exponent of Re_i is also consistent.

For $\mathrm{Re}_i > 1000$ (i.e., $\mathrm{Re}_i \gg 50$), we have $0.63\mathrm{Re}_i \gg 4.8\mathrm{Re}_i^{1/2}$, and so the second term in the bracket of Eq. (4.31)A can be neglected:

$$\left(0.63\mathrm{Re}_i + 4.8\mathrm{Re}_i^{1/2}\right)^{2/3} \approx \left(0.63\mathrm{Re}_i\right)^{2/3} \quad \text{for} \quad \mathrm{Re}_i > 1000 \tag{4.38}$$

The relative error of this approximation is within 15%. Thus, Eq. (4.31)A simplifies to:

$$\mathrm{Sh}_i = \frac{B_i}{2} 0.63^{2/3}\mathrm{Re}_i^{2/3}\mathrm{Sc}^{1/3} = 0.367 B_i \mathrm{Re}_i^{2/3}\mathrm{Sc}^{1/3} \quad \text{for} \quad \mathrm{Re}_i > 1000 \tag{4.39}$$

which results in $\kappa = 0.367 B_i$. Using these methodology and results, we next intend to extend the analysis to the case of suspensions, which is more relevant to our system of interest.

In the absence of free-stream turbulence, the mass transfer coefficient for homogeneous suspensions can be calculated by Eq. (4.5), which can be equivalently written as:

$$\mathrm{Sh}_L = \frac{B}{2}\left(0.63\mathrm{Re}_t + 4.8\mathrm{Re}_t^{1/2}\right)^{2/3}\mathrm{Sc}^{1/3} \quad ; \quad \mathrm{Re}_t \equiv \mathrm{Re}_i \alpha_e^{1-m} \tag{4.40}$$

As we see, if Re_t is replaced by Re_i, Eq. (4.40)A becomes identical to Eq. (4.31)A. Therefore, the conclusions drawn for isolated particles also apply to suspensions, except that the criterion is now based on Re_t instead of Re_i. For $\mathrm{Re}_t < 0.1$, the first term in the bracket of Eq. (4.40)A is negligible, and the expression below offers an accurate approximation, with a relative error within 3%:

$$\mathrm{Sh}_L = \frac{B}{2} 4.8^{2/3}\mathrm{Re}_t^{1/3}\mathrm{Sc}^{1/3} = 1.423 B \mathrm{Re}_t^{1/3}\mathrm{Sc}^{1/3} \quad \text{for} \quad \mathrm{Re}_t < 0.1 \tag{4.41}$$

So, $\kappa = 1.423 B$. For $10 < \mathrm{Re}_t < 1000$, the approximation below is valid, with a relative error within 15%:

$$\mathrm{Sh}_L = \frac{B}{2}(2 \cdot 2 \cdot 0.63 \cdot 4.8)^{1/3}\mathrm{Re}_t^{1/2}\mathrm{Sc}^{1/3} = 1.148 B \mathrm{Re}_t^{1/2}\mathrm{Sc}^{1/3} \quad \text{for} \quad 10 < \mathrm{Re}_t < 1000 \tag{4.42}$$

Therefore, $\kappa = 1.148 B$. For $0.1 < \mathrm{Re}_t < 10$, determining a single exponent for Re_t is challenging, and so a value for the parameter κ cannot be found. To address this, we examine the applicability of Eqs. (4.41) and (4.42) within this range. For $0.1 < \mathrm{Re}_t < 5$, Eq. (4.41) ($\kappa = 1.423 B$) provides a good approximation, while for $5 < \mathrm{Re}_t < 10$, Eq. (4.42) ($\kappa = 1.148 B$) is more accurate; in both cases, the relative error is within 15%. For $\mathrm{Re}_t > 1000$, the second term in the bracket of Eq. (4.40)A is negligible. The resulting approximation is:

$$\mathrm{Sh}_L = \frac{B}{2} 0.63^{2/3}\mathrm{Re}_t^{2/3}\mathrm{Sc}^{1/3} = 0.367 B \mathrm{Re}_t^{2/3}\mathrm{Sc}^{1/3}, \quad \mathrm{Re}_t > 1000 \tag{4.43}$$

with a relative error within 15%. Therefore, for this case, $\kappa = 0.367 B$. Note that in these expressions for κ, the value of B is not required, because it cancels out in Eq. (4.11); in any case, the values of B are known and are reported in Wang et al. [19].

Employing Eqs. (4.20) and (4.30) in the free-stream-turbulence models summarized in Table 2 and adopting the values for κ that we have just derived, $\langle \overline{\mathrm{Sh}} \rangle$ can be calculated via Eqs. (4.9), (4.11) and (4.40). This method allows accounting for the combined effect of fluid-particle slip velocity, particle interactions and free-stream turbulence (all calculated locally) on mass transfer.

4.2. Turbulent multifluid model

To use the proposed method, we must know the profiles of the fluid dynamic variables within the vessel, such as the phase averages of the mean velocities, the Reynolds averages of the volume fractions and the turbulent kinetic energies of the phases. In general, fluid dynamics is affected by mass transfer, because this alters the physical properties of the fluid, such as density and viscosity, as well as the particle size and the solid volume fraction. Hence, in liquid-particle agitated vessels where mass transfer takes place, the fluid dynamics is time dependent, making $\langle\overline{\mathrm{Sh}}\rangle$ vary with time (the time scale of this process is far larger than that characterizing the $\overline{\mathrm{Sh}}$ fluctuations). However, as discussed in Section 2.2, $\langle\overline{\mathrm{Sh}}\rangle$ is usually taken to be constant. This assumption is valid when the measurements are conducted over a sufficiently short time interval, so that variations in the fluid and particle properties, as well as in the solute concentration, are negligible. Conversely, assuming $\langle\overline{\mathrm{Sh}}\rangle$ to be constant during the entire dissolution process may lead to uncertainties, if measurements are made over the entire dissolution process [3,6,9,30,34,36,37,45]. We will assume that $\langle\overline{\mathrm{Sh}}\rangle$ is constant, so that it is reasonable to calculate the fluid dynamic variables by using the initial properties of the fluid and the particles. These variables can then be used in Eqs. (4.9) and (4.11) to calculate $\langle\overline{\mathrm{Sh}}\rangle$. In this study, the fluid dynamic variables are calculated via the turbulent multifluid model of Fox [50], which is briefly presented below. For details, see also Wang and Mazzei [51].

4.2.1. Governing equations

For the liquid phase, the Reynolds averaged continuity and dynamical equations read:

$$\partial_t\langle\alpha_e\rangle = -\partial_{\boldsymbol{x}}\cdot\langle\alpha_e\rangle\langle\boldsymbol{u}_e\rangle_E \tag{4.44}$$

$$\rho_e\partial_t(\langle\alpha_e\rangle\langle\boldsymbol{u}_e\rangle_E) = -\rho_e\partial_{\boldsymbol{x}}\cdot\langle\alpha_e\rangle\langle\boldsymbol{u}_e\rangle_E\langle\boldsymbol{u}_e\rangle_E - \partial_{\boldsymbol{x}}\cdot\langle\boldsymbol{S}_e\rangle - \partial_{\boldsymbol{x}}\cdot\boldsymbol{T}_e - \langle\boldsymbol{f}_p\rangle + \langle\alpha_e\rangle\rho_e\boldsymbol{g} \tag{4.45}$$

where $\boldsymbol{S}_e$ and $\boldsymbol{T}_e$ are the effective stress tensor and turbulent stress tensor for the fluid phase, respectively, and $\boldsymbol{f}_p$ is the mean fluid-particle interaction force. For the solid phase, the Reynolds averaged continuity and dynamical equations read:

$$\partial_t\langle\alpha_s\rangle = -\partial_{\boldsymbol{x}}\cdot\langle\alpha_s\rangle\langle\boldsymbol{u}_s\rangle_S \tag{4.46}$$

$$\rho_s\partial_t(\langle\alpha_s\rangle\langle\boldsymbol{u}_s\rangle_S) = -\rho_s\partial_{\boldsymbol{x}}\cdot\langle\alpha_s\rangle\langle\boldsymbol{u}_s\rangle_S\langle\boldsymbol{u}_s\rangle_S - \partial_{\boldsymbol{x}}\cdot\langle\boldsymbol{S}_s\rangle - \partial_{\boldsymbol{x}}\cdot\boldsymbol{T}_s + \langle\boldsymbol{f}_p\rangle + \langle\alpha_s\rangle\rho_s\boldsymbol{g} \tag{4.47}$$

where $\boldsymbol{S}_s$ and $\boldsymbol{T}_s$ are the effective stress tensor and turbulent stress tensor for the solid phase, respectively. At moderately large solid volume fractions, particle collisions significantly affect the solid phase effective stress tensor and in turn the fluid dynamics of the suspension. Thus, the set of balance equations for mass and linear momentum is complemented by a balance equation for the granular internal energy, $(3/2)\theta_s$, where θ_s is the granular temperature [52,53]. The Reynolds average of this equation reads:

$$\rho_s\partial_t[\langle\alpha_s\rangle(3/2)\langle\theta_s\rangle_S] = -\rho_s\partial_{\boldsymbol{x}}\cdot\langle\alpha_s\rangle(3/2)\langle\theta_s\rangle_S\langle\boldsymbol{u}_s\rangle_S - \partial_{\boldsymbol{x}}\cdot\boldsymbol{q}_{st} - \partial_{\boldsymbol{x}}\cdot\langle\boldsymbol{q}_s\rangle - \langle\boldsymbol{S}_s:\partial_{\boldsymbol{x}}\boldsymbol{u}_s\rangle - \langle S_c\rangle - \langle S_v\rangle \tag{4.48}$$

Here, $\boldsymbol{q}_s$ and $\boldsymbol{q}_{st}$ are the granular and turbulent heat fluxes, respectively. S_c and S_v are sink terms of granular internal energy owing to inelastic particle collisions and viscous resistance to particle motion.

As we see, these equations involve several undetermined terms. Details on their closures will be provided in the following section.

4.2.2. Closures

In this section, we present the closures for the undetermined terms. The constitutive equations as well as the associated parameter values used in our model and briefly presented below are those identified by Wang and Mazzei [51] as preferable for simulating liquid-particle turbulent flows in agitated vessels. Adopting the same multifluid model employed in this work, Wang and Mazzei [51] systematically examined the impact of different closures and of the values of their parameters – assigned within ranges commonly used in the literature – on the accuracy of the model predictions. Thus, we do not perform this analysis here, referring to their work for further details.

Most of the expressions given below are consistent with those found in Fox [50], to whom we refer for mathematical details; however, the notation and, more importantly, some closures are different. For instance, Fox assumes $\alpha_s\rho_s/\beta$ (that is, the drag time scale) to be a constant, where β is the drag coefficient, while we do not; in addition, for the effective viscosity of the fluid phase η_e, Fox uses the closure $\eta_e = \mu_e + \mu_e^\star$, where μ_e is the molecular viscosity of the fluid and $\mu_e^\star$ is a "pseudo-turbulent" viscosity accounting for the stress arising from the point fluid velocity fluctuations due, for instance, to particle wakes, while we use the expression $\eta_e = \alpha_e\mu_e$, which is commonly adopted in the literature [52]. $\langle\boldsymbol{S}_e\rangle$ is given by:

$$\langle\boldsymbol{S}_e\rangle = \langle p_e\rangle\boldsymbol{I} - \langle\eta_e\rangle[\partial_{\boldsymbol{x}}\langle\boldsymbol{u}_e\rangle_E + (\partial_{\boldsymbol{x}}\langle\boldsymbol{u}_e\rangle_E)^\dagger - (2/3)\partial_{\boldsymbol{x}}\cdot\langle\boldsymbol{u}_e\rangle_E\boldsymbol{I}] \tag{4.49}$$

where $\langle p_e\rangle$ is the mean pressure of the fluid phase (i.e., one third of the trace of $\langle\boldsymbol{S}_e\rangle$), $\langle\eta_e\rangle = \langle\alpha_e\rangle\mu_e$, and $\boldsymbol{I}$ is the unit tensor. $\langle\boldsymbol{S}_s\rangle$ is given by:

$$\langle\boldsymbol{S}_s\rangle = [\langle p_s\rangle - \langle\lambda_s\rangle\partial_{\boldsymbol{x}}\cdot\langle\boldsymbol{u}_s\rangle_S]\boldsymbol{I} - \langle\eta_s\rangle[\partial_{\boldsymbol{x}}\langle\boldsymbol{u}_s\rangle_S + (\partial_{\boldsymbol{x}}\langle\boldsymbol{u}_s\rangle_S)^\dagger - (2/3)\partial_{\boldsymbol{x}}\cdot\langle\boldsymbol{u}_s\rangle_S\boldsymbol{I}] \tag{4.50}$$

where the solid pressure $\langle p_s\rangle$, bulk viscosity $\langle\lambda_s\rangle$ and viscosity $\langle\eta_s\rangle$ are given by:

$$\langle p_s\rangle = \langle\alpha_s\rangle\rho_s\langle\theta_s\rangle_S + 2\langle\alpha_s\rangle^2\rho_s\langle\theta_s\rangle_S g_0(1+e) \quad ;$$

$$\langle\lambda_s\rangle = (4/3)\langle\alpha_s\rangle^2\rho_s d_p g_0(1+e)\sqrt{\langle\theta_s\rangle_S/\pi} \quad ;$$

$$\langle\eta_s\rangle = \frac{\langle\alpha_s\rangle\rho_s d_p\sqrt{\langle\theta_s\rangle_S\pi}}{6(3-e)}\left[1+\frac{2}{5}\langle\alpha_s\rangle g_0(1+e)(3e-1)\right] + \frac{3}{5}\langle\lambda_s\rangle \quad ;$$

$$g_0 = \left[1-\left(\frac{\langle\alpha_s\rangle}{\alpha_{s,max}}\right)^{1/3}\right]^{-1} \tag{4.51}$$

in which e is the restitution coefficient, g_0 is the radial distribution function, and $\alpha_{s,max}$ is the packing limit (often, as also here, set at 63%).

The turbulent stress tensor of the fluid phase $\boldsymbol{T}_e$ is closed using Boussinesq's eddy viscosity hypothesis; therefore, we write:

$$\boldsymbol{T}_e = (2/3)\langle\alpha_e\rangle\rho_e k_e\boldsymbol{I} - \langle\alpha_e\rangle\mu_{t,e}[\partial_{\boldsymbol{x}}\langle\boldsymbol{u}_e\rangle_E + (\partial_{\boldsymbol{x}}\langle\boldsymbol{u}_e\rangle_E)^\dagger - (2/3)\partial_{\boldsymbol{x}}\cdot\langle\boldsymbol{u}_e\rangle_E\boldsymbol{I}] \tag{4.52}$$

where $\mu_{t,e}$ is the turbulent viscosity of the fluid phase, given by:

$$\mu_{t,e} = C_{\mu e}\rho_e k_e^2/\varepsilon_e \tag{4.53}$$

where ε_e – not to be confused with the Kolmogorov eddy dissipation rate ε – is the dissipation rate of the fluid turbulent kinetic energy k_e, and $C_{\mu e}$ is a parameter, usually set equal to 0.09 [54–56]. The solid turbulent stress tensor $\boldsymbol{T}_s$ is closed with equations analogous to Eqs. (4.52) and (4.53), with k_e and ε_e replaced by k_s and ε_s, that is, the turbulent kinetic energy of the solid phase and its dissipation rate, respectively.

The fluid-particle interaction force $\langle\boldsymbol{f}_p\rangle$ comprises various contributors; the main ones are the buoyancy $\langle\boldsymbol{f}_{p,B}\rangle$ and the drag $\langle\boldsymbol{f}_{p,D}\rangle$ forces. Here, we only consider these [55,57–60]. For the buoyancy force, we use the following closure:

$$\langle\boldsymbol{f}_{p,B}\rangle = -\langle\alpha_s\rangle\partial_{\boldsymbol{x}}\langle p_e\rangle - C_p\langle\alpha_e\rangle\langle\alpha_s\rangle(\rho_s-\rho_e)\boldsymbol{g} \tag{4.54}$$

Here, C_p is a constant whose value should lie between zero to unity; following Wang and Mazzei [51], we set it to zero. The drag force is closed as follows:

$$\langle\boldsymbol{f}_{p,D}\rangle = \beta(\langle\boldsymbol{u}_e\rangle_E - \langle\boldsymbol{u}_s\rangle_S + \boldsymbol{u}_{dr}) \tag{4.55}$$

in which β is the drag force coefficient and $\boldsymbol{u}_{dr} \equiv \langle\alpha_s'\boldsymbol{u}_e''\rangle/(\langle\alpha_e\rangle\langle\alpha_s\rangle)$ is referred to as drift velocity. Various closures can be found for β. For

instance, see Jackson [53], Mazzei and Lettieri [61] and Marchisio and Fox [62] for reviews. Here, using the closure of Syamlal et al. [63], we write:

$$\beta = \frac{3}{4} C_D \frac{\langle \alpha_e \rangle \langle \alpha_s \rangle \rho_e}{\xi^2 d_p} |\langle \boldsymbol{u}_e \rangle_E - \langle \boldsymbol{u}_s \rangle_S| \tag{4.56}$$

where:

$$C_D = \left(0.63 + \frac{4.8}{\sqrt{\mathrm{Re}/\xi}}\right)^2 \quad ;$$

$$\xi = \frac{1}{2}\left[A - 0.06\mathrm{Re} + \sqrt{(0.06\mathrm{Re})^2 + 0.12(2B - A)\mathrm{Re} + A^2}\right] \quad ;$$

$$\mathrm{Re} \equiv \frac{|\langle \boldsymbol{u}_e \rangle_E - \langle \boldsymbol{u}_s \rangle_S| d_p}{\nu_e} \quad ; \quad A = \langle \alpha_e \rangle^{4.14} \quad ;$$

$$B = \begin{cases} 0.8\langle \alpha_e \rangle^{1.28} & \text{for } \langle \alpha_e \rangle \leq 0.85 \\ \langle \alpha_e \rangle^{2.65} & \text{for } \langle \alpha_e \rangle > 0.85 \end{cases} \tag{4.57}$$

In Eq. (4.55), the part of $\langle \boldsymbol{f}_{p,D} \rangle$ related to $\boldsymbol{u}_{dr}$ is referred to as turbulent dispersion force. Fox [50] closes $\boldsymbol{u}_{dr}$ as follows:

$$\boldsymbol{u}_{dr} = -\frac{\mu_{e,t}}{\langle \alpha_e \rangle \langle \alpha_s \rangle \rho_e \mathrm{Sc}_{es}} \partial_{\boldsymbol{x}} \langle \alpha_s \rangle - C_g (\langle \boldsymbol{u}_e \rangle_E - \langle \boldsymbol{u}_s \rangle_S) \quad ; \quad \mathrm{Sc}_{es} \equiv (k_e/k_s)^{1/2} \tag{4.58}$$

Here, Sc_{es} is the turbulent Schmidt number and $0 \leq C_g \leq 1$. As indicated by Fox [50], the second term on the right-hand side of Eq. (4.58)A is valid exclusively for cases where $\rho_e \ll \rho_s$. For liquid-particle systems, its expression may be inaccurate and may have to be modified (but no other closures are available). Following Wang and Mazzei [51], we neglect this term.

The granular heat flux featuring in Eq. (4.47) is expressed via Fourier's law, where the thermal conductivity is modeled using the closure of Syamlal et al. [63]. Therefore, we write:

$$\langle \boldsymbol{q}_s \rangle = -k_\theta \partial_{\boldsymbol{x}} \langle \theta_s \rangle_S \tag{4.59}$$

with:

$$k_\theta = \frac{15\langle \alpha_s \rangle \rho_s d_p \sqrt{\langle \theta_s \rangle_S \pi}}{4(41 - 33\zeta)} \times \left\{1 + \left[\frac{12}{5}\zeta^2(4\zeta - 3) + \frac{16}{15\pi}\zeta(41 - 33\zeta)\right]\langle \alpha_s \rangle g_0\right\} \tag{4.60}$$

where k_θ is the granular conductivity and $\zeta \equiv (1 + e)/2$. The closures for the sink terms related to inelastic collisions and to viscous resistance to the particle motions read:

$$\langle S_c \rangle = \frac{\langle \alpha_s \rangle \rho_s \langle \theta_s \rangle_S (1 - e^2)}{2\tau_s^c} \quad ; \quad \tau_s^c \equiv \frac{d_p}{24\langle \alpha_s \rangle g_0} \sqrt{\frac{\pi}{\langle \theta_s \rangle_S}} \quad ;$$

$$\langle S_v \rangle = 3\beta \langle \theta_s \rangle_S \tag{4.61}$$

The turbulent heat flux $\boldsymbol{q}_{st}$ is modeled by the gradient diffusion model, given by:

$$\boldsymbol{q}_{st} = -\frac{3}{2} \frac{\langle \alpha_s \rangle \mu_{t,s}}{\mathrm{Pr}_{es}} \partial_{\boldsymbol{x}} \langle \theta_s \rangle_S \tag{4.62}$$

where Pr_{es} is the turbulent Prandtl number, whose value ranges from 0.5 to 0.9 [54]; here, we take it to be 0.85. The fourth term on the right-hand side of Eq. (4.48) is expressed as follows:

$$\langle \boldsymbol{S}_s : \partial_{\boldsymbol{x}} \boldsymbol{u}_s \rangle = \langle \boldsymbol{S}_s \rangle : \partial_{\boldsymbol{x}} \langle \boldsymbol{u}_s \rangle_S - \langle \alpha_s \rangle \rho_s \varepsilon_s \tag{4.63}$$

The closures reported above require knowledge of the turbulent kinetic energy and of its dissipation rate for both phases. To obtain these fields, we have to solve their transport equations. For the fluid turbulent kinetic energy, the equation reads:

$$\rho_e \partial_t (\langle \alpha_e \rangle k_e) = -\rho_e \partial_{\boldsymbol{x}} \cdot \langle \alpha_e \rangle k_e \langle \boldsymbol{u}_e \rangle_E + \partial_{\boldsymbol{x}} \cdot \left(\langle \eta_e \rangle + \frac{\langle \alpha_e \rangle \mu_{t,e}}{\sigma_{e,k}}\right) \partial_{\boldsymbol{x}} k_e - \boldsymbol{T}_e : \partial_{\boldsymbol{x}} \langle \boldsymbol{u}_e \rangle_E - \langle \alpha_e \rangle \rho_e \varepsilon_e + \Pi_{k,e} + \Pi_{k,ep} + \Pi_{k,e\rho} \tag{4.64}$$

Here, $\sigma_{e,k}$ is a constant, assigned to be unity [54]. $\Pi_{k,e}$, $\Pi_{k,ep}$ and $\Pi_{k,e\rho}$ are the source terms owing to the turbulent interaction between the phases, the gradient of the Reynolds-averaged fluid pressure, and the covariance of the fluctuations of the mean fluid velocity and fluid pressure gradient, respectively. We follow Fox [50] and close these terms as:

$$\Pi_{k,e} = \beta\{2[\Psi_k (k_e k_s)^{1/2} - k_e] - (\langle \boldsymbol{u}_e \rangle_E - \langle \boldsymbol{u}_s \rangle_S) \cdot \boldsymbol{u}_{dr}\} \quad ;$$

$$\Pi_{k,ep} = \langle \alpha_s \rangle \boldsymbol{u}_{dr} \cdot \partial_{\boldsymbol{x}} \langle p_e \rangle \quad ;$$

$$\Pi_{k,e\rho} = C_\rho \langle \alpha_s \rangle (\rho_s - \rho_e) \boldsymbol{u}_{dr} \cdot \boldsymbol{g} \tag{4.65}$$

in which Ψ_k and C_ρ are constants, taken to be unity [56]. The transport equation for the rate of dissipation of the fluid turbulent kinetic energy reads:

$$\rho_e \partial_t (\langle \alpha_e \rangle \varepsilon_e) = -\rho_e \partial_{\boldsymbol{x}} \cdot \langle \alpha_e \rangle \varepsilon_e \langle \boldsymbol{u}_e \rangle_E + \partial_{\boldsymbol{x}} \cdot \left(\langle \eta_e \rangle + \frac{\langle \alpha_e \rangle \mu_{t,e}}{\sigma_{e,\varepsilon}}\right) \partial_{\boldsymbol{x}} \varepsilon_e - \frac{\varepsilon_e}{k_e}(C_1 \boldsymbol{T}_e : \partial_{\boldsymbol{x}} \langle \boldsymbol{u}_e \rangle_E + C_2 \langle \alpha_e \rangle \rho_e \varepsilon_e) + \Pi_{\varepsilon,e} + \frac{\varepsilon_s}{k_s}(C_4 \Pi_{k,ep} + C_5 \Pi_{k,e\rho}) \tag{4.66}$$

where:

$$\Pi_{\varepsilon,e} = \beta\left\{2C_3[\Psi_\varepsilon (\varepsilon_e \varepsilon_s)^{1/2} - \varepsilon_e] - C_4 \frac{\varepsilon_s}{k_s}(\langle \boldsymbol{u}_e \rangle_E - \langle \boldsymbol{u}_s \rangle_S) \cdot \boldsymbol{u}_{dr}\right\} \tag{4.67}$$

is a source term owing to the turbulent interaction between the phases. C_1 to C_5, $\sigma_{e,\varepsilon}$ and Ψ_ε are constants. C_1 and C_2 are taken to be 1.44 and 1.92, respectively, $\sigma_{e,\varepsilon}$ is taken to be 1.3 [54], whilst the other four constants are taken to be unity [56]. The transport equation for the solid turbulent kinetic energy reads:

$$\rho_s \partial_t (\langle \alpha_s \rangle k_s) = -\rho_s \partial_{\boldsymbol{x}} \cdot \langle \alpha_s \rangle k_s \langle \boldsymbol{u}_s \rangle_S + \partial_{\boldsymbol{x}} \cdot \left(\langle \eta_s \rangle + \frac{\langle \alpha_s \rangle \mu_{t,s}}{\sigma_{s,k}}\right) \partial_{\boldsymbol{x}} k_s - \boldsymbol{T}_s : \partial_{\boldsymbol{x}} \langle \boldsymbol{u}_s \rangle_S - \langle \alpha_s \rangle \rho_s \varepsilon_s + \Pi_{k,s} + \Pi_{k,s\rho} \tag{4.68}$$

$\sigma_{s,k}$ is set to unity [54]. $\Pi_{k,s}$ and $\Pi_{k,s\rho}$ are source terms owing to the turbulent interaction between the two phases and the covariance of the fluctuations of the mean solid velocity and fluid pressure gradient, respectively. Their closures are:

$$\Pi_{k,s} = 2\beta[\Psi_k (k_e k_s)^{1/2} - k_s] \quad ;$$

$$\Pi_{k,s\rho} = -C_\rho C_p \langle \alpha_e \rangle \langle \alpha_s \rangle (\rho_s - \rho_e)(\langle \boldsymbol{u}_e \rangle_E - \langle \boldsymbol{u}_s \rangle_S) \cdot \boldsymbol{g} - \Pi_{k,e\rho} \tag{4.69}$$

The transport equation for the solid turbulent kinetic energy dissipation rate reads:

$$\rho_s \partial_t (\langle \alpha_s \rangle \varepsilon_s) = -\rho_s \partial_{\boldsymbol{x}} \cdot \langle \alpha_s \rangle \varepsilon_s \langle \boldsymbol{u}_s \rangle_S + \partial_{\boldsymbol{x}} \cdot \left(\langle \eta_s \rangle + \frac{\langle \alpha_s \rangle \mu_{t,s}}{\sigma_{s,\varepsilon}}\right) \partial_{\boldsymbol{x}} \varepsilon_s - \frac{\varepsilon_s}{k_s}(C_1 \boldsymbol{T}_s : \partial_{\boldsymbol{x}} \langle \boldsymbol{u}_s \rangle_S + C_2 \langle \alpha_s \rangle \rho_s \varepsilon_s) + \Pi_{\varepsilon,s} + C_5 \frac{\varepsilon_s}{k_s} \Pi_{k,s\rho} \tag{4.70}$$

$\sigma_{s,\varepsilon}$ is taken to be 1.3 [54], and $\Pi_{\varepsilon,s}$, caused by the turbulent interaction between the phases, is given by the following equation:

$$\Pi_{\varepsilon,s} = 2C_3 \beta[\Psi_\varepsilon (\varepsilon_e \varepsilon_s)^{1/2} - \varepsilon_s] \tag{4.71}$$

The balance equations and closures just shown are solved with the CFD software Fluent. For agitated vessels with a rotating impeller, the sliding mesh (SM) and multiple reference frame (MRF) numerical methods are commonly used. In baffled vessels, like those considered here, the relative position between the impeller and the baffles changes continuously, resulting in an inherently unsteady flow. But after an initial transient period, the flow becomes periodic. The SM method can capture both the transient and periodic evolutions of the fluid dynamic variables and mass transfer coefficients with high accuracy, but is quite demanding computationally and therefore impractical. Nevertheless, the time scales associated with the onset of the periodic flow and of the subsequent flow oscillations are far smaller than that relevant to mass transfer measurements. Thus, such variations typically do not manifest in the experimentally measured values of the mass transfer coefficient

$\overline{k}$. Under these conditions, the MRF method can yield approximate, but usually sufficiently good, solutions at a far lower computational cost [58,60,64]. Therefore, in this study we adopt this method. Once the profiles of the Reynolds averages of the volume fractions, of the phase averages of the mean velocities, and of the turbulent properties are obtained, we calculate $\langle\overline{\mathrm{Sh}}\rangle$ via Eqs. (4.9), (4.11), (4.20), (4.30) and (4.40). In the next section, we will apply this method to some selected experimental studies and examine its applicability by comparing the predictions with experimental data.

5. Results and discussion

In the previous section, we have developed a new method for calculating the globally averaged mass transfer coefficient in agitated vessels; this first predicts the fluid dynamic variables employing the multifluid model described in Section 4.2, and then uses these variables in Eqs. (4.9), (4.11), (4.20), (4.30) and (4.40) to calculate $\langle\overline{\mathrm{Sh}}\rangle$. In Section 5.1, we validate this method by applying it to selected experiments and comparing predictions with experimental data. Furthermore, in Section 5.2, we compare the predictions of our method with those from the approaches discussed in Section 3.2.

5.1. Method validation

To validate the method, we employ the experimental data on globally averaged mass transfer coefficients of Barker and Treybal [3], Nienow [36], Nienow [37], and Bong [40], details of which can be found in Table 1. Barker and Treybal [3] and Bong [40] measured the change in solute concentration and calculated $\overline{k}$ using Eq. (2.5). In the latter study, ion exchange beads were used, making the assumptions of constant d_p and α_s reasonable. In the former study, dissolving particles were used, but the authors estimated the mass transfer coefficient at the initial stage, where only a small fraction of the particles dissolves; this reduces the uncertainties introduced by assuming d_p, α_s and $\overline{k}$ to be constant. Nevertheless, since both studies overlooked the factor $1/(1-\overline{\alpha}_{s,0})$, their data must be modified. In contrast, Nienow [36,37] measured either the remaining solid mass during the dissolution process or the time for complete particle dissolution and estimated the value of $\overline{k}$ with Eq. (2.9). Among these four studies, the selected data cover a broad range of conditions: the solid volume fraction varies between 0.6% and 40%, Sc between 650 and $4.12\cdot10^4$, the particle diameter between 0.67 and 2.86 mm, and the density difference between the particles and the liquid between 198 and 1660 kg/m^3. These wide ranges ensure the generality of the validation. From these studies, we only consider data from cylindrical flat-bottomed baffled vessels equipped with six-blade disc turbines, because these systems are commonly used and well-characterized. But it is important to emphasize that the proposed methodology is not inherently limited to any particular vessel or impeller type. Our method is general, and the accuracy of the results depends primarily on the ability of the multifluid model presented in Section 4.2 to accurately predict the fluid dynamics in the vessel (and on the accuracy of the constitutive equations). As demonstrated in Wang and Mazzei [51], the multifluid model has also been validated for vessels equipped with six-blade 45° pitched blade turbines, further supporting the generalizability of the proposed approach to other system configurations. Information about the numerical schemes and techniques used in the simulations, as well as initial and boundary conditions, are provided in Appendix A and Appendix B.

For the selected experiments, to estimate the value of Pe_i within the vessel, in Eq. (4.6)B we replace the locally volume-averaged velocities ($\boldsymbol{u}_e$ and $\boldsymbol{u}_s$) with their respective (ensemble) phase averages ($\langle\boldsymbol{u}_e\rangle$ and $\langle\boldsymbol{u}_s\rangle$). Using the values of these velocities obtained via the multifluid model, we find that the values of Pe_i are on the order of 10^3 or larger; hence, the concentration boundary layer theory is applicable, and Eq. (4.11) can be adopted without including the term for mass transfer under zero flow conditions.

As discussed, to account for the effect of free-stream turbulence on mass transfer, we employ the models summarized in Table 2, with Re_i and T_i calculated with Eqs. (4.20) and (4.30), respectively. Fig. 1 compares the predicted values of $\langle\overline{\mathrm{Sh}}\rangle$ with the experimental data. The predictions without considering the free-stream turbulence effect are also reported, where instead of Eq. (4.11), $\langle\mathrm{Sh}_L\rangle_S$ is calculated as:

$$\langle\mathrm{Sh}_L\rangle_S = \mathrm{Sh}_L(\langle\alpha_e\rangle, \mathrm{Re}_i, \mathrm{Sc}) \tag{5.1}$$

with Re_i defined as per Eq. (4.20). As seen, accounting for free-stream turbulence generally yields higher $\langle\overline{\mathrm{Sh}}\rangle$ values. This aligns with the expectation that free-stream turbulence should enhance mass transfer. However, the values of $\langle\overline{\mathrm{Sh}}\rangle$ obtained from the various free-stream-turbulence models differ significantly. For the data of Barker and Treybal [3], reported in Fig. 1(a), the model that performs best is that by Lavender and Pei [21], followed by those of Sandoval-Robles et al. [25] and Gostkowski and Costello [24]; for those of Nienow [36], shown in Fig. 1(b), the best models, which perform equally well, are those by Lavender and Pei [21] and Galloway and Sage [23], followed by that of Gostkowski and Costello [24]; for the data of Nienow [37], reported in Fig. 1(c), again the model that performs best is that by Lavender and Pei [21], followed by those of Gostkowski and Costello [24] and Sandoval-Robles et al. [25]; finally, for the data of Bong [40], shown in Fig. 1(d), the best model is that by Lavender and Pei [21], followed by those of Gostkowski and Costello [24] and Galloway and Sage [23]. Therefore, at least for the 72 experimental data considered in this study, the model that in general performs best is that by Lavender and Pei [21].

When the model by Lavender and Pei [21] is employed, for most data the relative percent error between the predicted and experimental values is less than 30%. This good alignment validates our proposed method, showing that it applies not only when $\overline{k}$ is measured over a short time interval, as done by Barker and Treybal [3] and implicitly in our method, but also when the coefficient (assumed to be constant) is measured over relatively long ion exchange or dissolution processes, as done by Nienow [36,37] and Bong [40]. The discrepancies between the predictions and the measurements may arise from several factors. First, the closures used in the turbulent multifluid model might introduce some inaccuracies in the predicted fluid dynamics variables (see Wang and Mazzei [51]). Second, the correlation of Wang et al. [19] adopted to calculate the local mass transfer coefficient (Eq. (4.5)) is also affected by error (the authors reporting that, for most cases, it is less than 30%). Third, the models that we used to account for the effect of free-stream turbulence on the mass transfer of fixed isolated particles and their extension to cases where both liquid and particles move and a large number of particles is involved are also expected to cause uncertainties. Finally, for the experimental data, no error bars are available, and the assumptions made to calculate the mass transfer coefficients, such as assuming uniform and constant particle size for dissolving particles and a constant mass transfer coefficient when measurements span relatively extended mass transfer processes (see Section 2.2), may also contribute to the discrepancies.

5.2. Comparison with other methods

In this section, we compare the predictions of our method with those of other methods. The correlations used for this comparison are shown in Table 3. As discussed in Section 3.2, several methods have been proposed for estimating the globally averaged mass transfer coefficient in agitated vessels. Among these, correlations derived directly for $\overline{k}$ using dimensional analysis are typically case-specific and cannot be generalized when experimental conditions change, so in our comparison these correlations are not considered.

For approaches based on the steady-state theory, which neglects the effect of free-stream turbulence, we consider only the method proposed

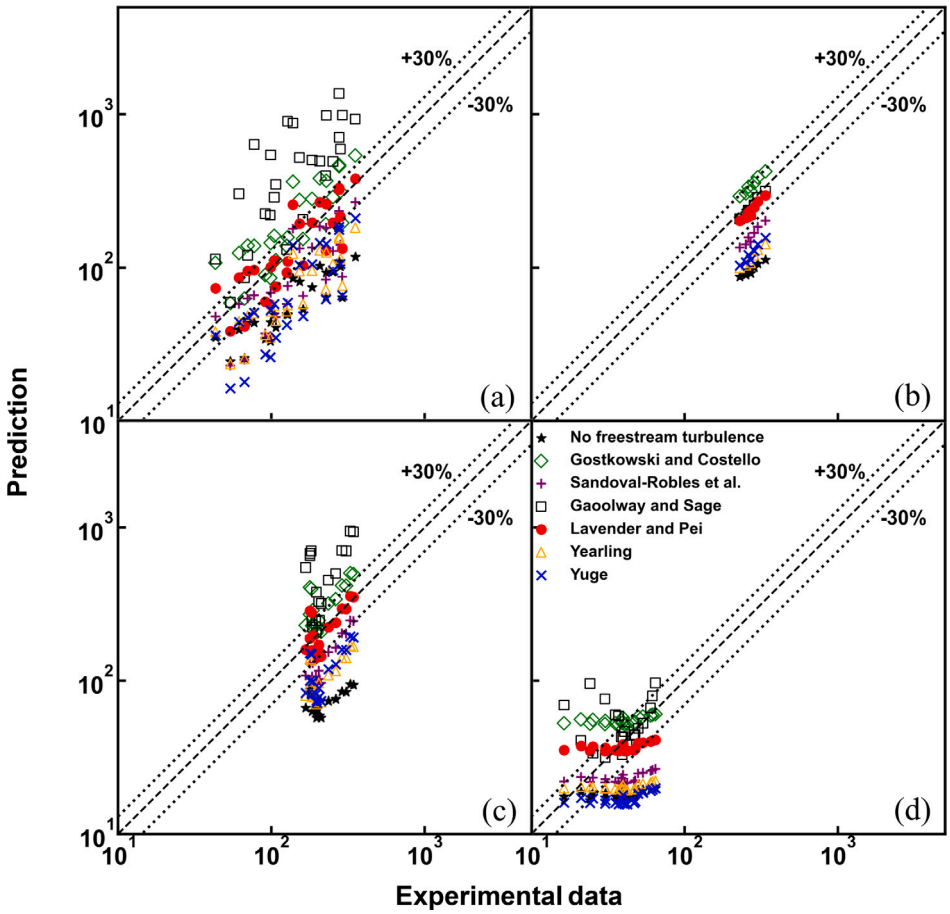

Fig. 1. Comparisons between predictions and experimental data on $\langle \overline{\mathrm{Sh}} \rangle$ for experiments from (a) Barker and Treybal [3], (b) Nienow [36], (c) Nienow [37] and (d) Bong [40] with various models for the effect of free-stream turbulence.

by Kuboi et al. [10]; this assumes a constant mass transfer coefficient for all the particles in the vessel, and to predict $\overline{k}$ it applies correlations developed for isolated particles, such as those by Friedlander [14] and Frossling [13]. This method requires a value for $u_{r,i}$ (see Eq. (3.5)C); to estimate it, we adopt the approach proposed by Kuboi et al. [10], who, for data where $d_p \gg \eta$, related $u_{r,i}$ to the average Kolmogorov eddy dissipation rate $\overline{\varepsilon}$, writing:

$$\mathrm{Re}_i = \mathrm{Re}_{\overline{\varepsilon}}/2 \quad ; \quad \mathrm{Re}_i \equiv u_{r,i} d_p/\nu_e \quad ; \quad \mathrm{Re}_{\overline{\varepsilon}} \equiv \overline{\varepsilon}^{1/3} d_p^{4/3}/\nu_e \tag{5.2}$$

Accordingly, we use this approximation (reported to have an accuracy within ±50%) and substitute Re_i with $\mathrm{Re}_{\overline{\varepsilon}}/2$ in the relevant correlations in Table 3.

To account for free-stream turbulence, Kuboi et al. [10] and Armenante and Kirwan [30] adopted the penetration theory. We exclude the correlation by Armenante and Kirwan [30], insofar as their experiments involved particles with $d_p \ll \eta$. In the model by Kuboi et al. [10], a constant mass transfer coefficient is assumed for the all particles, enabling the use of Eq. (3.5)A for calculating the globally averaged value. Since Eq. (3.5) depends on $u_{r,i}$, we again use Eq. (5.2) for its estimation and substitute Re_i with $\mathrm{Re}_{\overline{\varepsilon}}/2$ in the relevant correlations in Table 3. For the correlations based on the Kolmogorov theory, we omit those by Armenante and Kirwan [30] and Bong et al. [34]; the former is excluded for the same reason mentioned before, and the latter involves parameters (see Eq. (3.15)) that are unknown. Consequently, only the correlation by Calderbank and Moo-Young [31] is considered in our comparison.

As shown, all the correlations for the comparison require $\overline{\varepsilon}$. This is generally taken to be equal to P/M_e, where P is the power input and M_e is the total mass of the liquid in the vessel. The power input is commonly calculated using the empirical expression [30,32]:

$$P = N_p \rho_e N^3 d_I^5 \tag{5.3}$$

where N_p is the power number. For baffled vessels with a six-blade disk turbine, and for the conditions of the selected experiments, N_p is generally assumed constant, and here we adopt the value 5.6 [3,34,40].

Fig. 2 compares the predictions of the correlations reported in Table 3 with the experimental data from Barker and Treybal [3], Nienow [36,37] and Bong [40]. Note that for these experimental data, the Reynolds number values, calculated using Eq. (5.2)A, are consistently greater than unity. Therefore, for the models based on the steady-state theory, only the correlation similar to that proposed by Frossling [13] is applied. When free-stream turbulence is neglected, most of the experimental data are significantly underestimated. A similar underestimation is evident for the correlation derived from the Kolmogorov theory. Because $2/\sqrt{\pi} \approx 1$, the two correlations derived from the penetration theory give very similar predictions; a slight overestimation is observed for the data from Nienow [36,37], while the overestimation is more pronounced for the data from Barker and Treybal [3] and Bong [40].

Table 3
Correlations considered in the comparison with our method.

Theory	Correlation for $\langle \overline{Sh} \rangle$	Reference
Steady-state theory	$2 + 0.552 Re_i^{1/2} Sc^{1/3}$ for $Re_i > 1$ $2 + 0.991 (Re_i\, Sc)^{1/3}$ for $Re_i < 1$	Kuboi et al. [10]
Unsteady-state theory	$2 + \frac{2}{\sqrt{\pi}} Re_i^{1/2} Sc^{1/2}$ (constant) $2 + Re_i^{1/2} Sc^{1/2}$ (random)	Kuboi et al. [10]
Kolmogorov theory	$0.13 Re_{\bar{\varepsilon}}^{3/4} Sc^{1/3}$	Calderbank and Moo-Young [31]

'constant' and 'random' represent constant and random exposure time distributions, respectively.

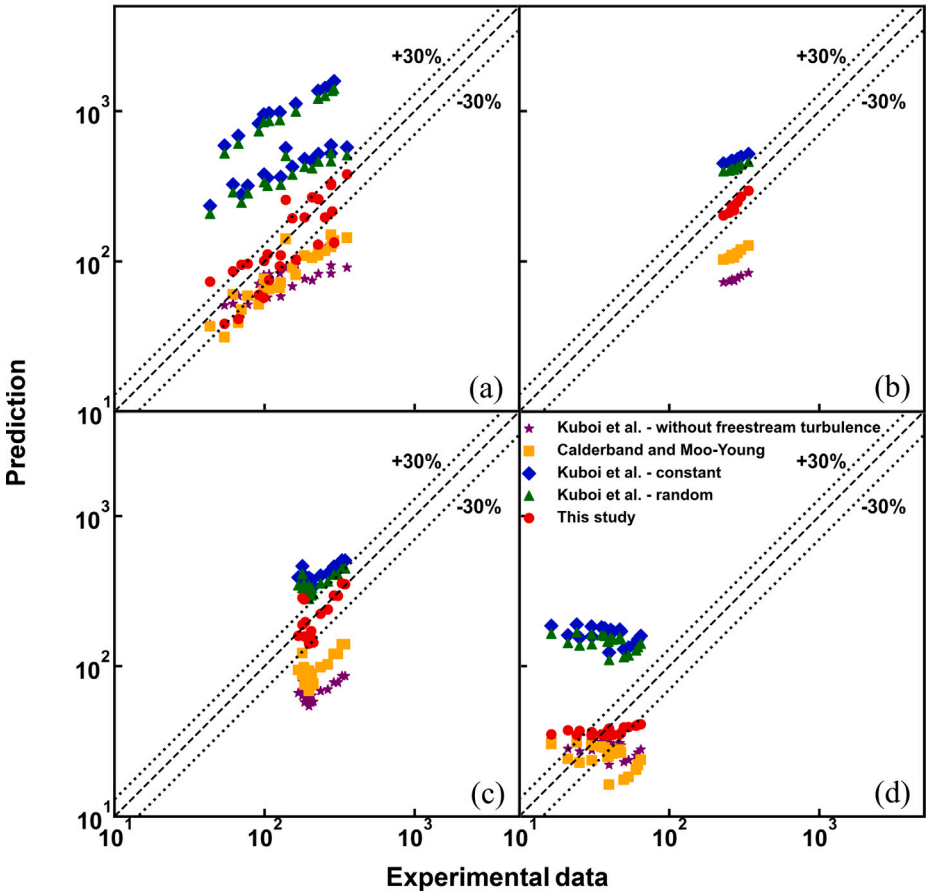

Fig. 2. Comparisons between the predictions of various methods and experimental data on $\langle \overline{Sh} \rangle$ for experiments from (a) Barker and Treybal [3], (b) Nienow [36], (c) Nienow [37] and (d) Bong [40] with $Re_i = Re_{\bar{\varepsilon}}/2$ ('constant' and 'random' represent constant and random exposure time distributions, respectively).

Notice that replacing Re_i with $Re_{\bar{\varepsilon}}/2$ involves an uncertainty of up to ±50% [10]. To evaluate the sensitivity of the model predictions to this approximation, we consider two other formulations: $Re_i = Re_{\bar{\varepsilon}}/3$ and $Re_i = Re_{\bar{\varepsilon}}$. In both cases, the Reynolds number values remain larger than unity, and thus for the models based on the steady-state theory, only the correlation similar to that proposed by Frossling [13] is used. The corresponding predictions are presented in Figs. 3 and 4, respectively. As shown, for the correlation without free-stream turbulence, the experimental data are still underestimated except for those from Barker and Treybal [3] and Bong [40] when $Re_i = Re_{\bar{\varepsilon}}$. When penetration theory is used, the predictions for the data of Nienow [36] and Nienow [37] show good agreement when $Re_i = Re_{\bar{\varepsilon}}/3$ is assumed, whereas adopting $Re_i = Re_{\bar{\varepsilon}}$ results in a notable overestimation. Conversely, for the data of Barker and Treybal [3] and Bong [40], both expressions of Re_i lead to significant overestimations.

In summary, the predictions of the available methods generally exhibit larger deviations from the measured data – most exceeding 30% – than those obtained using the method developed in this study, which highlights the improvement of the proposed approach. These relatively large discrepancies in the existing methods may arise from several factors. First, neglecting free-stream turbulence leads to consistent underestimation. When its effect is considered, correlations developed for isolated particles are used directly for multiparticle systems, overlooking the effect of particle interactions on mass transfer; furthermore,

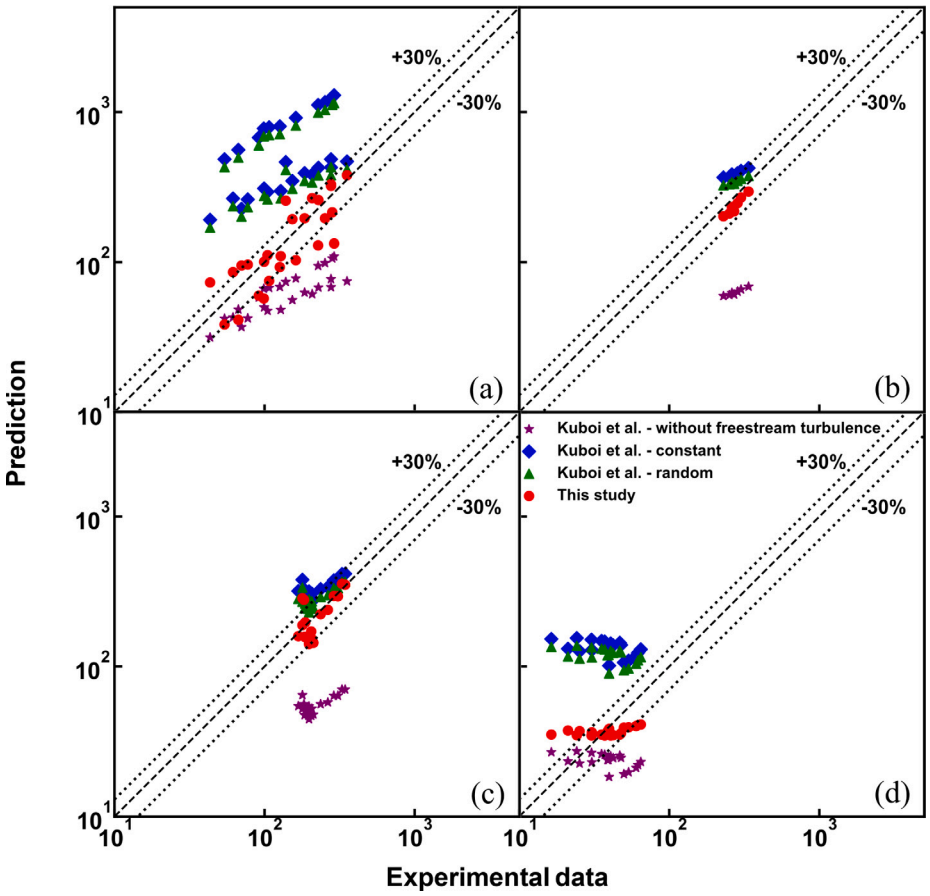

Fig. 3. Comparisons between the predictions of various methods and experimental data on $\langle\overline{\mathrm{Sh}}\rangle$ for experiments from (a) Barker and Treybal [3], (b) Nienow [36], (c) Nienow [37] and (d) Bong [40] with $\mathrm{Re}_i = \mathrm{Re}_{\overline{\varepsilon}}/3$ ('constant' and 'random' represent constant and random exposure time distributions, respectively).

the assumption of an equal mass transfer coefficient for all particles and the use of $\overline{\varepsilon}$ introduce additional inaccuracies. In contrast, our method achieves better agreement with the experimental data by accounting for the combined effects of fluid-particle slip velocity, particle interactions and free-stream turbulence (all calculated locally) on mass transfer.

5.3. A final remark

As discussed in Section 4, the method developed for calculating the globally averaged mass transfer coefficient refers to the case in which all the particles dispersed in the vessel have the same size; moreover, the particle size is assumed to be constant. About the first assumption (i.e., particles of equal size), this can be easily relaxed, but the simulations would become more demanding computationally. To this end, one would have to generalize the multifluid model and the method for the calculation of the mass transfer coefficients by considering many particle classes, each comprising particles of equal size (considering a continuous particle size distribution is also possible, but this would require the implementation of a population balance equation, which would render the simulations even more time consuming). The generalization would not be complex; for instance, Eq. (4.4) would turn into:

$$\overline{\mathrm{Sh}} = \sum_{r=1}^{\nu}\left[\left(\frac{\overline{d}_p}{d_{p,r}}\right)^2\left(\frac{\overline{\alpha}_{s,r,0}}{\overline{\alpha}_{s,0}}\right)\right]\overline{\mathrm{Sh}}_r \quad ; \quad \overline{\mathrm{Sh}}_r = \frac{1}{\overline{\alpha}_{s,r,0}V_V}\int_{V_V}\alpha_{s,r}\mathrm{Sh}_{L,r}dV \tag{5.4}$$

where ν is the number of particle classes, $\overline{d}_p \equiv 6\overline{\alpha}_{s,0}V_V/A_V$ is the globally averaged particle diameter, $d_{p,r}$ is the diameter of the particles belonging to class r, $\overline{\alpha}_{s,r,0}$ is the globally averaged volume fraction of these particles, and $\alpha_{s,r}$ is their local volume fraction. For these particles, the local Sherwood number $\mathrm{Sh}_{L,r}$ would still be calculated using Eq. (4.5).

Also the second assumption (i.e., constant particle size) can be relaxed; for each particle class, the change in particle size would have to be captured through the relevant mass balance equation, which should feature a mass transfer term involving the instantaneous local mass transfer coefficient. Therefore, one would have to modify the multifluid model, but not the method for calculating the mass transfer coefficients. But since for each particle class, the particle size would change differently in different spatial locations, a finite number of particle classes (each with fixed particle size) would not suffice; hence, a continuous particle size distribution would have to be considered, and a population balance equation (PBE) would have to be solved for the solid phase. In a CFD code, the PBE could be solved with a quadrature-based method; this method would model the continuous particle size distribution through a finite number of classes – but in each class the particle size would be a function of the time and space coordinates, hence allowing the nonuniform mass transfer process to be accurately described. For further details about this method, we refer to the literature (e.g., [62,65–68]).

6. Conclusions

This study developed a new method for calculating the globally averaged mass transfer coefficient in agitated vessels. This method adopts a turbulent multifluid model to predict the fluid dynamic variables in

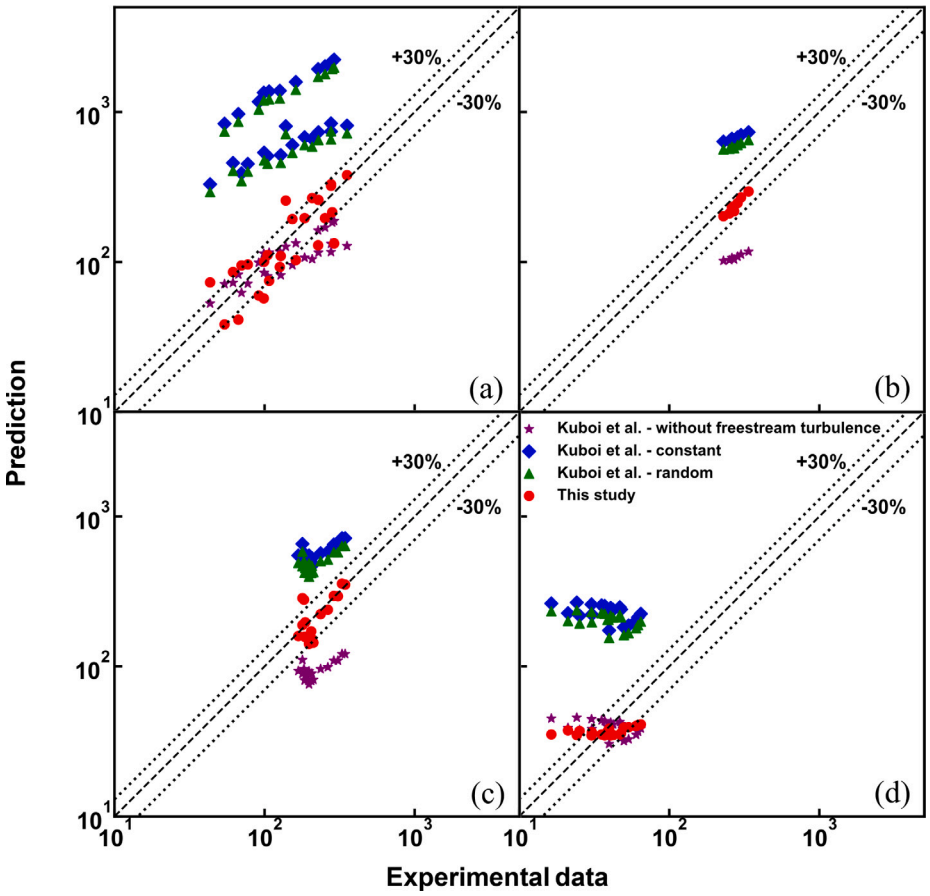

Fig. 4. Comparisons between the predictions of various methods and experimental data on $\langle\overline{\mathrm{Sh}}\rangle$ for experiments from (a) Barker and Treybal [3], (b) Nienow [36], (c) Nienow [37] and (d) Bong [40] with $\mathrm{Re}_i = \mathrm{Re}_{\bar{\varepsilon}}$ ('constant' and 'random' represent constant and random exposure time distributions, respectively).

the vessel and incorporates these results into a global-mass-transfer-coefficient model which accounts for the combined effects of fluid-particle slip velocity, particle interactions and free-stream turbulence.

The applicability and accuracy of the method were investigated by comparing its results to experimental data from Barker and Treybal [3], Nienow [36], Nienow [37] and Bong [40], over a wide range of experimental conditions. If an appropriate model for the effect of free-stream turbulence is adopted (in this study, the model of Lavender and Pei [21]), for most data points the relative percent error is within 30%. The discrepancies between results and experimental data can be attributed to several factors, such as the approximations involved in the closures of the turbulent multifluid model, the assumptions in the calculation of the mass transfer coefficients, and the uncertainties in the experimental measurements.

Comparatively, the available methods exhibit larger deviations due to their inherent assumptions, such as the use of correlations for isolated particles, the assumption of identical mass transfer coefficients for all the particles, and the neglect of the contribution of free-stream turbulence.

Notation

a	Constant	–
A_i	Surface area of particle i	m^2
A_L	Particle surface area per unit volume	m^2
A_T	Function of Re_i and T_i	–
A_V	Total surface area of the particles	m^2
A_1	Constant	–
A_2	Constant	–
b	Constant	–
b_1	Constant	–
b_2	Constant	–
b_3	Constant	–
B	Constant	–
B_i	Constant	–
c	Constant	–
C	Locally averaged solute concentration	kg/m^3
$\overline{C}$	Globally averaged solute concentration	kg/m^3
C_c	Constant	–
$\overline{C}_d$	Globally averaged solute concentration assuming complete dissolution	kg/m^3
C_D	Particle drag force coefficient	–
C_I	Impeller clearance	m
C_g	Constant	–
C_p	Constant	–
C_s	Saturation concentration at the particle surface	kg/m^3

$\overline{C}_0$	Globally averaged solute concentration at time zero	kg/m^3
$C_{\mu e}$	Constant	–
$\overline{C}_\tau$	Globally averaged solute concentration at time τ	kg/m^3
C_ρ	Constant	–
C_1	Constant	–
C_2	Constant	–
C_3	Constant	–
C_4	Constant	–
C_5	Constant	–
dM/dt	Local mass transfer rate per unit volume	kg/(m^3 s)
dM_V/dt	Global mass transfer rate	kg/s
$\mathscr{D}$	Solute diffusivity	m^2/s
$\mathscr{D}_t$	Turbulent diffusivity	m^2/s
d	Distance between two points	m
d_I	Impeller diameter	m
d_p	Particle diameter	m
$\overline{d}_p$	Globally averaged particle size	m
$d_{p,0}$	Particle diameter at time zero	m
$d_{p,j}$	Size of the particles belonging to class j	m
d_V	Vessel diameter	m
e	Restitution coefficient	–
$\boldsymbol{f}_p$	Mean fluid-particle interaction force	kg m/s^2
$\boldsymbol{f}_{p,B}$	Buoyancy force	kg m/s^2
$\boldsymbol{f}_{p,D}$	Drag force	kg m/s^2
g	Gravitational acceleration	m/s^2
g_0	Radial distribution function	–
Ga	Galilei number	–
H	Liquie height	m
$\boldsymbol{I}$	Unit tensor	–
$\overline{k}$	Globally averaged mass transfer coefficient	m/s
k_e	Turbulent kinetic energy of the fluid phase	m^2/s^2
k_i	Mass transfer coefficient of particle i	m/s
k_L	Locally averaged mass transfer coefficient	m/s
k_s	Turbulent kinetic energy of the solid phase	m^2/s^2
k_τ	Mean mass transfer coefficient of a single liquid element over its exposure period	m/s
k_θ	Granular conductivity	W/(m K)
L_i	Turbulence integral length scale	–
m	Richardson-Zaki exponent	–
M_s	Total particle mass	kg
$M_{s,i}$	Mass of particle i	kg
$M_{s,0}$	Total particle mass at time zero	kg
$M_{s,\tau}$	Total particle mass at time τ	kg
N	Impeller rotation speed	rps
N_p	Power number	–
p	Constant	–
$\boldsymbol{P}$	Power input	W
p_e	Pressure of the fluid phase	kg/(m s^2)
Pe$_i$	Particle Peclet number	–
Pr$_{es}$	Turbulent Prandtl number	–
p_s	Solid pressure	kg/(m s^2)
q	Constant	–
$\boldsymbol{q}_s$	Granular heat flux	W/m^2
$\boldsymbol{q}_{st}$	Turbulent heat flux	W/m^2
Re	Reynolds number	–
Re$_d$	Reynolds number based on particle diameter	–
Re$_i$	Reynolds number for particle i	–
Re$_I$	Reynolds number based on impeller diameter	–
Re$_t$	Reynolds number based on particle terminal velocity	–
Re$_V$	Reynolds number based on vessel diameter	–
Re$_\varepsilon$	Reynolds number based on ε	–
Re$_{\overline{\varepsilon}}$	Reynolds number based on $\overline{\varepsilon}$	–
Sc	Schmidt number	–
S_c	Sink term of granular internal energy owing to inelastic particle collisions	kg/(m s^3)
Sc$_{es}$	Turbulent Schmidt number	–
$\boldsymbol{S}_e$	Effective stress tensor for the fluid phase	kg/(m s^2)
$\overline{\mathrm{Sh}}$	Globally averaged Sherwood number	–
Sh$_i$	Sherwood number for particle i	–
$\overline{\mathrm{Sh}}_j$	Globally averaged Sherwood number for particle class j	–
Sh$_L$	Locally averaged Sherwood number	–
Sh$_{L,j}$	Locally averaged Sherwood number for particle class j	–
$\overline{\mathrm{Sh}}_V$	Sherwood number characterized by vessel diameter	–
$\boldsymbol{S}_s$	Effective stress tensor for the solid phase	kg/(m s^2)
S_v	Sink term of granular internal energy owing to viscous resistance to particle motion	kg/(m s^3)
$\boldsymbol{T}_e$	Turbulent stress tensor for the fluid phase	kg/(m s^2)
T$_i$	Turbulence intensity	–
$\boldsymbol{T}_s$	Turbulent stress tensor for the solid phase	kg/(m s^2)
u'	Root mean square of the relative velocity between two points in a turbulent flow	m/s
$\boldsymbol{u}_{dr}$	Drift velocity	m/s
$\boldsymbol{u}_e$	Locally averaged velocity for the fluid phase	m/s
$\bar{\boldsymbol{u}}_e$	Instantaneous velocity of the fluid in the free stream	m/s
$\bar{\boldsymbol{u}}_{e,1}$	Instantaneous velocities of the fluid at one point	m/s
$\bar{\boldsymbol{u}}_{e,2}$	Instantaneous velocities of the fluid at one point	m/s
$\bar{\boldsymbol{u}}_{p,i}$	Instantaneous velocity of particle i	m/s
$u_{r,i}$	Slip velocity between the fluid and particle i	m/s
$\bar{\boldsymbol{u}}_{r,i}$	Instantaneous velocity of approach of the fluid in the free stream	m/s
$\boldsymbol{u}_s$	Locally averaged velocity of the solid phase	m/s
u_t	Particle terminal velocity	m/s
v	Constant	–
V_e	Total volume of the fluid	m^3
V_V	Total volume of the suspension	m^3
y_s	Dimensionless concentration	–
y_τ	Dimensionless concentration at time τ	–

Greek symbols

α_e	Fluid volume fraction	–
α_s	Solid volume fraction	–
$\alpha_{s,j}$	Volume fraction for particle class j	–
$\alpha_{s,max}$	Packing limit of the solid phase	–
$\overline{\alpha}_s$	Globally averaged solid volume fraction	–
$\overline{\alpha}_{s,j,0}$	Globally averaged volume fraction of particle class j	–
$\overline{\alpha}_{s,0}$	Globally averaged solid volume fraction at time zero	–
$\overline{\alpha}_{s,\tau}$	Globally averaged solid volume fraction at time τ	–
β	Drag coefficient	kg/(m^3 s)
ε	Kolmogorov eddy dissipation rate of the surrounding fluid	m^2/s^3
ε_e	Turbulent kinetic energy dissipation rate of the fluid phase	m^2/s^3
ε_s	Turbulent kinetic energy dissipation rate of the solid phase	m^2/s^3
$\overline{\varepsilon}$	Globally averaged dissipation rate	m^2/s^3
η	Kolmogorov length scale	m
η_e	Effective viscosity of the fluid phase	Pa s
η_s	Effective viscosity of the solid phase	Pa s
θ_s	Granular temperature	m^2/s^2
κ	Constant	–
Λ	Average exposure time of the fluid elements	s
λ_s	Bulk viscosity of the solid phase	Pa s
μ_e	Viscosity of the fluid phase	Pa s
$\mu_e^\star$	"pseudo-turbulent" viscosity of the fluid phase	Pa s
$\mu_{t,e}$	Turbulent viscosity of the fluid phase	Pa s
$\mu_{t,s}$	Turbulent viscosity of the solid phase	Pa s
ν_e	Kinematic viscosity of the fluid phase	m^2/s
ζ	A generic locally averaged (or Eulerian) variable	–
$\langle\zeta\rangle$	Reynolds average of ζ	–
$\langle\zeta\rangle_E$	Fluid average of ζ	–
$\langle\zeta\rangle_S$	Solid average of ζ	–
ζ'	Fluctuating quantity corresponding to $\langle\zeta\rangle$	–
ζ''	Fluctuating quantity corresponding to $\langle\zeta\rangle_E$	–
ζ'''	Fluctuating quantity corresponding to $\langle\zeta\rangle_S$	–
$\Pi_{k,e}$	Source term to the fluid phase turbulent kinetic energy owing to the turbulent interaction between the phases	m^2/s^3
$\Pi_{k,ep}$	Source term to the fluid phase turbulent kinetic energy owing to the gradient of the Reynolds-averaged fluid pressure	m^2/s^3
$\Pi_{k,e\rho}$	Source term to the fluid phase turbulent kinetic energy owing to the covariance of the fluctuations of the mean fluid velocity and fluid pressure gradient	m^2/s^3
$\Pi_{k,s}$	Source term to the solid phase turbulent kinetic energy owing to the turbulent interaction between the two phases	m^2/s^3
$\Pi_{k,s\rho}$	Source term to the solid phase turbulent kinetic energy owing to the covariance of the fluctuations of the mean solid velocity and fluid pressure gradient	m^2/s^3
$\Pi_{\varepsilon,e}$	Source term to the fluid phase turbulent kinetic energy dissipation rate owing to the turbulent interaction between the phases	m^2/s^4
$\Pi_{\varepsilon,s}$	Source term to the solid phase turbulent kinetic energy dissipation rate owing to the turbulent interaction between the phases	m^2/s^4
ρ_e	Fluid density	kg/m^3
ρ_s	Particle density	kg/m^3
$\sigma_{e,k}$	Constant	–
$\sigma_{e,\varepsilon}$	Constant	–
$\sigma_{s,k}$	Constant	–
$\sigma_{s,\varepsilon}$	Constant	–
τ	Time	s
τ_e	Exposure time	s
ψ	Parameter related to the initial solid volume fraction	–
Ψ	Constant	1/m
Ψ_k	Constant	–
Ψ_ε	Constant	–

CRediT authorship contribution statement

Ziming Wang: Writing – original draft, Visualization, Validation, Software, Methodology, Investigation, Formal analysis, Data curation, Conceptualization. **Luca Mazzei:** Writing – review & editing, Supervision, Resources, Project administration, Methodology, Investigation, Funding acquisition, Formal analysis, Conceptualization.

Declaration of competing interest

The authors declare the following financial interests/personal relationships which may be considered as potential competing interests: Luca Mazzei reports financial support was provided by GlaxoSmithKline (GSK). Luca Mazzei reports a relationship with GlaxoSmithKline (GSK) that includes: funding grants. If there are other authors, they declare that they have no known competing financial interests or personal relationships that could have appeared to influence the work reported in this paper.

Acknowledgments

Funding from GlaxoSmithKline (UK) is gratefully acknowledged.

Appendix A. Boundary and initial conditions

Closed vessels were employed by Barker and Treybal [3] and Nienow [37]; for such vessels, no-slip boundary conditions are applied for both the fluid and solid phases at every wall, including the top wall. In contrast, open-top vessels were employed by Nienow [36] and Bong [40]. However, due to the presence of baffles, the gas–liquid interface is almost flat; hence, it is modeled as a flat surface with zero shear stress for both liquid and solid phases. This allows disregarding the flow in the gas phase, simplifying the simulations considerably. For all the considered cases, the surfaces of the rod and impeller are treated as rotating moving walls, while all the remaining walls are treated as stationary; on all the walls, no-slip boundary conditions are applied to both phases. Finally, the initial conditions assume a uniform distribution of motionless particles in a still liquid.

Appendix B. Numerical schemes and techniques

Unstructured tetrahedral meshes are adopted to discretize the flow domain. For the selected experiments, the vessel diameter ranges from 0.14 m to 0.3 m, while the vessel height is either equal to or approximately equal to the diameter. The number of mesh cells employed for these vessels is approximately 10^6, which falls within or exceeds the typical range reported in previous studies using similar vessel sizes [51,60,64]. For pressure-velocity coupling, the phase-coupled SIMPLE scheme is employed. For spatial discretization, the least squares cell based method is used for gradient calculations, and the PRESTO! method is used for pressure; owing to the complexity of the fluid model and the flow conditions, a first-order upwind scheme is used for momentum, volume fraction, turbulent kinetic energy and turbulent dissipation rates to ensure stability and convergence [69–71]. The Multiple Reference Frame (MRF) method is adopted in conjunction with a transient solver, with time steps ranging from 0.0001 s to 0.00025 s. Each time step is considered converged when all the residuals fall below 10^{-3}. Once the predicted fluid dynamic variables, such as volume fractions, velocities and turbulent properties, become nearly constant, the flow is considered to have reached a periodic state. During this periodic regime, even if the variables vary only slightly, time-averaged results over several seconds are used to calculate the mass transfer coefficient.

Data availability

Data will be made available on request.

References

[1] A.W. Hixson, S.J. Baum, Agitation. Mass transfer coefficients in liquid-solid agitation systems, Ind. Eng. Chem. 33 (4) (1941) 478–485.
[2] D. Humphrey, H. Van Ness, Mass transfer in a continuous-flow mixing vessel, AIChE J. 3 (2) (1957) 283–286.
[3] J.J. Barker, R.E. Treybal, Mass transfer coefficients for solids suspended in agitated liquids, AIChE J. 6 (2) (1960) 289–295.
[4] S. Nagata, I. Yamaguchi, S. Yabuta, M. Harada, Mass transfer in agitated liquid-solid systems, Mem. Fac. Eng. Kyoto Univ. 22 (1) (1960) 86–122.
[5] J. Marangozis, A. Johnson, A correlation of mass transfer data of solid-liquid systems in agitated vessels, Can. J. Chem. Eng. 40 (6) (1962) 231–237.
[6] P. Sykes, A. Gomezplata, Particle liquid mass transfer in stirred tanks, Can. J. Chem. Eng. 45 (4) (1967) 189–196.
[7] S. Boon-Long, C. Laguerie, J. Couderc, Mass transfer from suspended solids to a liquid in agitated vessels, Chem. Eng. Sci. 33 (7) (1978) 813–819.
[8] R.B. Bird, W.E. Stewart, E.N. Lightfoot, Transport Phenomena, John Wiley & Sons, 2002.
[9] P. Harriott, Mass transfer to particles: Part I. Suspended in agitated tanks, AIChE J. 8 (1) (1962) 93–101.
[10] R. Kuboi, I. Komasawa, T. Otake, M. Iwasa, Fluid and particle motion in turbulent dispersion-III: Particle-liquid hydrodynamics and mass-transfer in turbulent dispersion, Chem. Eng. Sci. 29 (3) (1974) 659–668.
[11] H. Hartmann, J. Derksen, H. Van den Akker, Numerical simulation of a dissolution process in a stirred tank reactor, Chem. Eng. Sci. 61 (9) (2006) 3025–3032.
[12] T. Hormann, D. Suzzi, J.G. Khinast, Mixing and dissolution processes of pharmaceutical bulk materials in stirred tanks: experimental and numerical investigations, Ind. Eng. Chem. Res. 50 (21) (2011) 12011–12025.
[13] N. Frossling, Uber die verdunstung fallernder tropfen, Gerlands Beitrage Zur Geophys. 52 (1938) 170–216.
[14] S. Friedlander, Mass and heat transfer to single spheres and cylinders at low Reynolds numbers, AIChE J. 3 (1) (1957) 43–48.
[15] C.M. Tchen, Mean Value and Correlation Problems Connected with the Motion of Particles Suspended in a Turbulent Fluid, Nijhoff, 1947.
[16] M. Satish, J. Zhu, Flow resistance and mass transfer in slow non-Newtonian flow through multiparticle systems, J. Appl. Mech. (1992) 431–437.
[17] P.K. Agarwal, Transport phenomena in multi-particle systems—II. Particle-fluid heat and mass transfer, Chem. Eng. Sci. 43 (9) (1988) 2501–2510.
[18] F. Scala, Particle-fluid mass transfer in multiparticle systems at low Reynolds numbers, Chem. Eng. Sci. 91 (2013) 90–101.
[19] Z. Wang, C. Christodoulou, L. Mazzei, Analytical study on the liquid-particle mass transfer coefficient for multiparticle systems, Chem. Eng. J. (2024) 152733.
[20] M.C. Smith, A.M. Kuethe, Effects of turbulence on laminar skin friction and heat transfer, Phys. Fluids (1966).
[21] W.J. Lavender, D.C. Pei, The effect of fluid turbulence on the rate of heat transfer from spheres, Int. J. Heat Mass Transfer 10 (4) (1967) 529–539.
[22] T. Yuge, Experiments on heat transfer of spheres, report 3 (influence of free-stream turbulence at higher Reynolds numbers), Rep. Inst. High Speed Mech. Jpn. 11 (1959) 209–230.
[23] T. Galloway, B. Sage, Thermal and material transfer in turbulent gas streams—A method of prediction for spheres, Int. J. Heat Mass Transfer 7 (3) (1964) 283–291.
[24] V.J. Gostkowski, F.A. Costello, The effect of free stream turbulence on the heat transfer from the stagnation point of a sphere, Int. J. Heat Mass Transfer 13 (8) (1970) 1382–1386.
[25] J. Sandoval-Robles, H. Delmas, J. Couderc, Influence of turbulence on mass transfer between a liquid and a solid sphere, AIChE J. 27 (5) (1981) 819–823.
[26] P.R.A. Yearling, Experimental Determination of Convective Heat and Mass Transfer Rates from Single Evaporating Liquid Droplets in a Turbulent Air Flow, North Carolina State University, 1995.
[27] P. Danckwerts, Significance of liquid-film coefficients in gas absorption, Ind. Eng. Chem. 43 (6) (1951) 1460–1467.
[28] P. Harriott, A review of mass transfer to interfaces, Can. J. Chem. Eng. 40 (2) (1962) 60–69.
[29] R. Kuboi, I. Komasawa, T. Otake, Fluid and particle motion in turbulent dispersion—II: Influence of turbulence of liquid on the motion of suspended particles, Chem. Eng. Sci. 29 (3) (1974) 651–657.
[30] P.M. Armenante, D.J. Kirwan, Mass transfer to microparticles in agitated systems, Chem. Eng. Sci. 44 (12) (1989) 2781–2796.
[31] P. Calderbank, M.B. Moo-Young, The continuous phase heat and mass-transfer properties of dispersions, Chem. Eng. Sci. 16 (1–2) (1961) 39–54.
[32] D. Levins, J. Glastonbury, Application of Kolmogorofff's theory to particle—liquid mass transfer in agitated vessels, Chem. Eng. Sci. 27 (3) (1972) 537–543.
[33] J. Davies, Particle suspension and mass transfer rates in agitated vessels, Chem. Eng. Process.: Process. Intensif. 20 (4) (1986) 175–181.
[34] E.Y. Bong, N. Eshtiaghi, J. Wu, R. Parthasarathy, Optimum solids concentration for solids suspension and solid–liquid mass transfer in agitated vessels, Chem. Eng. Res. Des. 100 (2015) 148–156.
[35] A. Hixson, G. Wilkens, Performance of agitators in liquid-solid chemical systems, Ind. Eng. Chem. 25 (11) (1933) 1196–1203.
[36] A. Nienow, Dissolution mass transfer in a turbine agitated baffled vessel, Can. J. Chem. Eng. 47 (3) (1969) 248–258.
[37] A. Nienow, Agitated vessel particle-liquid mass transfer: a comparison between theories and data, Chem. Eng. J. 9 (2) (1975) 153–160.
[38] P. Lal, S. Kumar, S.N. Upadhyay, Y.D. Upadhya, Solid-liquid mass transfer in agitated Newtonian and non-Newtonian fluids, Ind. Eng. Chem. Res. 27 (7) (1988) 1246–1259.
[39] S.V. Jadhav, V.G. Pangarkar, Particle-liquid mass transfer in mechanically agitated contactors, Ind. Eng. Chem. Res. 30 (11) (1991) 2496–2503.
[40] E.Y. Bong, Solid-Liquid Mass Transfer in Agitated Vessels with High Solids Concentration (Ph.D. thesis), RMIT University, 2013.
[41] C. Carletti, S. Bikic, G. Montante, A. Paglianti, Mass transfer in dilute solid–liquid stirred tanks, Ind. Eng. Chem. Res. 57 (18) (2018) 6505–6515.
[42] G. Montante, C. Carletti, F. Maluta, A. Paglianti, Solid dissolution and liquid mixing in turbulent stirred tanks, Chem. Eng. Technol. 42 (8) (2019) 1627–1634.
[43] R. Mattern, O. Bilous, E.L. Piret, Continuous-flow stirred tank reactors: Solid-liquid systems, AIChE J. 3 (4) (1957) 497–505.
[44] H. Cao, C. Amador, X. Jia, Y. Li, Y. Ding, A modelling framework for bulk particles dissolving in turbulent regime, Chem. Eng. Res. Des. 114 (2016) 108–118.
[45] F. Grisafi, A. Brucato, G. Caputo, S. Lima, F. Scargiali, Modelling particle dissolution in stirred vessels, Chem. Eng. Res. Des. 195 (2023) 662–672.
[46] E. Ruckenstein, A note concerning turbulent exchange of heat or mass with a boundary, Chem. Eng. Sci. 7 (4) (1958) 265–268.
[47] T.J. Hanratty, Turbulent exchange of mass and momentum with a boundary, AIChE J. 2 (3) (1956) 359–362.
[48] G. Astarita, Mass Transfer with Chemical Reaction, Elsevier, 1967.
[49] L. Xie, Q. Wang, X. Luo, Z. Luo, CFD simulation of the particle dispersion behavior and mass transfer–reaction kinetics in non-newton fluid with high viscosity, Int. J. Chem. React. Eng. 17 (7) (2019) 20180293.
[50] R.O. Fox, On multiphase turbulence models for collisional fluid–particle flows, J. Fluid Mech. 742 (2014) 368–424.
[51] Z. Wang, L. Mazzei, A critical analysis of multifluid turbulent models for simulating liquid–particle turbulent flows in agitated vessels, Chem. Eng. Res. Des. 219 (2025) 52–66.
[52] D. Gidaspow, Multiphase Flow and Fluidization: Continuum and Kinetic Theory Descriptions, Academic Press, 1994.
[53] R. Jackson, The Dynamics of Fluidized Particles, Cambridge University Press, 2000.
[54] D.C. Wilcox, et al., Turbulence Modeling for CFD, vol. 2, DCW industries La Canada, CA, 1998.

[55] X. Shan, G. Yu, C. Yang, Z.-S. Mao, W. Zhang, Numerical simulation of liquid-solid flow in an unbaffled stirred tank with a pitched-blade turbine downflow, Ind. Eng. Chem. Res. 47 (9) (2008) 2926–2940.
[56] M. Riella, R. Kahraman, G.R. Tabor, Reynolds-Averaged Two-Fluid model prediction of moderately dilute fluid-particle flow over a backward-facing step, Int. J. Multiph. Flow 106 (2018) 95–108.
[57] M. Ljungqvist, A. Rasmuson, Numerical simulation of the two-phase flow in an axially stirred vessel, Chem. Eng. Res. Des. 79 (5) (2001) 533–546.
[58] D. Wadnerkar, R.P. Utikar, M.O. Tade, V.K. Pareek, CFD simulation of solid–liquid stirred tanks, Adv. Powder Technol. 23 (4) (2012) 445–453.
[59] A. Tamburini, A. Cipollina, G. Micale, A. Brucato, M. Ciofalo, Influence of drag and turbulence modelling on CFD predictions of solid-liquid suspensions in stirred vessels, Chem. Eng. Res. Des. 92 (6) (2014) 1045–1063.
[60] D. Wadnerkar, M.O. Tade, V.K. Pareek, R.P. Utikar, CFD simulation of solid–liquid stirred tanks for low to dense solid loading systems, Particuology 29 (2016) 16–33.
[61] L. Mazzei, P. Lettieri, A drag force closure for uniformly dispersed fluidized suspensions, Chem. Eng. Sci. 62 (22) (2007) 6129–6142.
[62] D.L. Marchisio, R.O. Fox, Computational Models for Polydisperse Particulate and Multiphase Systems, in: Cambridge Series in Chemical Engineering, Cambridge University Press, 2013.
[63] M. Syamlal, W. Rogers, T.J. O'Brien, MFIX Documentation Theory Guide, Technical Note, DOE/METC, 94, 1993, p. 1.
[64] F. Maluta, A. Paglianti, G. Montante, RANS-based predictions of dense solid–liquid suspensions in turbulent stirred tanks, Chem. Eng. Res. Des. 147 (2019) 470–482.
[65] D.L. Marchisio, R.O. Fox, Multiphase Reacting Flows: Modelling and Simulation, Springer Vienna, 2007.
[66] L. Mazzei, Eulerian Modelling and Computational Fluid Dynamics Simulation of Mono and Polydisperse Fluidized Suspensions (ProQuest Dissertations and Theses Global), University College London, 2008.
[67] L. Mazzei, Limitations of quadrature-based moment methods for modeling inhomogeneous polydisperse fluidized powders, Chem. Eng. Sci. 66 (16) (2011) 3628–3640.
[68] L. Mazzei, Segregation dynamics of dense polydisperse fluidized suspensions modeled using a novel formulation of the direct quadrature method of moments, Chem. Eng. Sci. 101 (2013) 565–576.
[69] Y. Shen, B. Qin, X. Li, Z. Zhu, P. Cui, J. Gao, Y. Wang, Investigation of the flow characteristics of liquid–liquid two-phase mixing in an agitator equipped with a "V-shaped" horizontal baffle, Environ. Dev. Sustain. 23 (2021) 2298–2313.
[70] A. Ashraf, B. Kumar, V.S.T. Madana, Experimental and computational investigation of solid suspension and gas dispersion in a stirred vessel, Phys. Fluids 34 (11) (2022).
[71] E. Phumnok, P. Saetiao, P. Bumphenkiattikul, S. Rattanawilai, P. Khongprom, CFD simulation of silica dispersion/natural rubber latex mixing for high silica content rubber composite production, RSC Adv. 14 (18) (2024) 12612–12623.